University of Alberta

Holocene Loess-Soil Deposits in Siberia: Geophysical and Geological Parameters as Regional and Global Climate Indicators

by

Shawn Douglas Walker

©

A thesis submitted to the Faculty of Graduate Studies and Research
in partial fulfillment of the requirements for the degree of

Master of Science
in
Geophysics

Department of Physics

Edmonton, Alberta
Spring 2008

Library and Archives Canada

Published Heritage Branch

395 Wellington Street
Ottawa ON K1A 0N4
Canada

Bibliothèque et Archives Canada

Direction du Patrimoine de l'édition

395, rue Wellington
Ottawa ON K1A 0N4
Canada

Your file Votre référence
ISBN: 978-0-494-45903-4
Our file Notre référence
ISBN: 978-0-494-45903-4

NOTICE:
The author has granted a non-exclusive license allowing Library and Archives Canada to reproduce, publish, archive, preserve, conserve, communicate to the public by telecommunication or on the Internet, loan, distribute and sell theses worldwide, for commercial or non-commercial purposes, in microform, paper, electronic and/or any other formats.

The author retains copyright ownership and moral rights in this thesis. Neither the thesis nor substantial extracts from it may be printed or otherwise reproduced without the author's permission.

AVIS:
L'auteur a accordé une licence non exclusive permettant à la Bibliothèque et Archives Canada de reproduire, publier, archiver, sauvegarder, conserver, transmettre au public par télécommunication ou par l'Internet, prêter, distribuer et vendre des thèses partout dans le monde, à des fins commerciales ou autres, sur support microforme, papier, électronique et/ou autres formats.

L'auteur conserve la propriété du droit d'auteur et des droits moraux qui protège cette thèse. Ni la thèse ni des extraits substantiels de celle-ci ne doivent être imprimés ou autrement reproduits sans son autorisation.

In compliance with the Canadian Privacy Act some supporting forms may have been removed from this thesis.

While these forms may be included in the document page count, their removal does not represent any loss of content from the thesis.

Conformément à la loi canadienne sur la protection de la vie privée, quelques formulaires secondaires ont été enlevés de cette thèse.

Bien que ces formulaires aient inclus dans la pagination, il n'y aura aucun contenu manquant.

Canada

Abstract

Holocene wind-blown sediments of Siberia could potentially provide an important link between Northern Atlantic and South Asian climatic fluctuations during the last thousands of years. Nothing is known about their relevance to regional and global climatic periodicity recorded in lacustrine and oceanic sediments and ice caps. We carried out extensive sampling of three Holocene loess/soil sections in the centre of continental Asia (along the Selenga River valley). Relative wind strength was determined by grain size analyses of different stratigraphic units. Petromagnetic measurements were performed to provide a proxy for the relative extent of pedogenesis. An age model for the sections was supported by detailed stratigraphic description and radiocarbon dating.

The windy events are associated with the absence of soil formation and relatively low values of frequency dependence of magnetic susceptibility (FD) that appeared to be an excellent quantitative marker of pedogenic activity. These events correspond to cold intervals registered in Lake Baikal sediments characterized by very low productivity of diatomaceous water plants. Periods where the strength of the wind was low are characterized by soil formation and correspond to high FD values in the studied loess sections and high diatom productivity intervals in Lake Baikal sediments. Our results demonstrate periodic change in relatively warm and cold intervals during the Holocene of Siberia that also may be associated with North Atlantic near millennial-scale climate cyclicity.

Table of Contents

Chapter 1 – Introduction.....1

Chapter 2 – Study Sites.....9

Chapter 3 – Methodology.....14
Field Methods.....14
Testing Methods and Equipment.....14

Chapter 4 – Stratigraphy and Sedimentology.....19
Burdukovo – Trench 1.....19
Unit 16: 0.00 m – 1.19 m.....19
Unit 15: 1.19 m – 1.48 m.....22
Unit 14: 1.48 m – 1.80 m.....22
Unit 13: 1.80 m – 2.25 m.....23
Unit 12: 2.25 m – 2.50 m.....23
Unit 11: 2.50 m – 3.20 m.....24
Unit 3: 3.20 m – 4.05 m.....25
Burdukovo – Trench 3.....25
Unit 16: 0.00 m – 0.46 m.....25
Unit 15: 0.46 m – 0.83 m.....26
Unit 11: 0.83 m – 1.03 m.....26
Unit 10: 1.03 m – 1.24 m.....27
Unit 9: 1.24 m – 1.44 m.....27
Unit 8: 1.44 m – 1.61 m.....28
Unit 7: 1.61 m – 2.02 m.....28
Unit 6: 2.02 m – 2.36 m.....29
Unit 5: 2.36 m – 2.68 m.....29
Unit 4: 2.36 m – 2.68 m.....30
Unit 3: 2.68 m – 3.45 m.....30
Burdukovo – Trench 4.....31
Unit 16: 0.00 m – 0.70 m.....31
Unit 15: 0.70 m – 1.18 m.....32
Unit 11: 1.18 m – 1.59 m.....33
Unit 5: 1.59 m – 1.95 m.....34
Unit 4: 1.95 m – 2.06 m.....35
Unit 3: 2.06 m – 3.25 m.....35
Unit 2: 3.25 m – 4.12 m.....36
Unit 1: 4.12 m – 4.40 m.....37

Chapter 5.1 – Age Model.....40

Chapter 5.2 – Magnetic Susceptibility and Grain Size Analysis.....45

Chapter 5.3 – Magnetic Mineralogy.....54

Chapter 5.4 – Correlation of Regional and Global Holocene Data.....61

Chapter 5.5 – Spectral Analysis.....66

Chapter 6 – Discussion.....72

Chapter 7 – Conclusions.....76

Bibliography.....77

Appendix - Data Tables.....81

Chapter 1 Introduction

Loess/paleosol sequences are wind blown deposits that can be found around the world (figure 1.1). They have been used as climate indicators for the Holocene and Pleistocene because of their sensitivity to their depositional environment. Loess is a deposit of sediment that has been transported to the depositional site via wind activity. Because it is transported and deposited through wind activity, the grain sizes found in loess deposits are usually less than 70 μm. This is because the transport strength of wind is not enough to transport larger materials. A loess unit is formed during colder, windier, and drier periods when the rate of deposition increases and the rate of pedogenesis, or soil forming processes, are suppressed. Soil units are formed during periods where the climate is warmer and moister and the wind strength is weaker (Evans and Heller, 2003). The soil at the Burdukovo site start out as wind blown sediment, but due to lower depositional rates and increased pedogenesis during warmer climes, the soil forming processes outstrip deposition and the sediment is transformed into a soil unit. These conditions give direction when looking for parameters to characterize depositional conditions. Grain sizes are a characteristic that can be used as a proxy for wind strength because, as the wind strength increases, so does the size of particles that can be entrained by the wind (Bagnold, 1941). For a typical loess/soil sequence, such as the classical Chinese loess deposits (Liu et al., 1988), the soil units show a higher magnetic susceptibility (figure 1.2). This is produced during pedogenesis as bacteria break down larger material, such as goethite or limonite, into superparamagnetic magnetite (Evans and Heller, 2003). There are several biological processes occurring, including the formation of magnetosomes (Balkwill et al., 1980) and the use of iron oxides as a source of energy which results in

Figure 1.1 Location of loess deposits worldwide (redrawn from Evans and Heller, 2003). The green dots in (A) Alaska (Muhs et al., 2004) and (B) Iceland (Jackson et al., 2005) represent Holocene loess deposits from other studies. The red dot (C) is the location of the Holocene loess deposit that is used for this study.

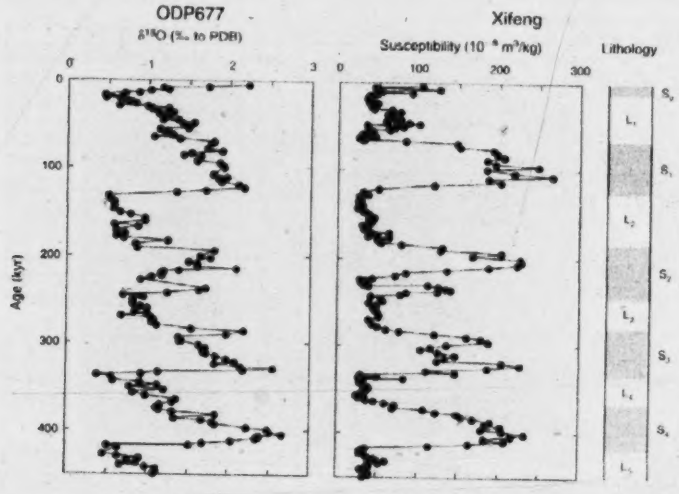

Figure 1.2 A typical loess/soil sequence showing positive correlation where soil units display a high magnetic susceptibility and loess a low susceptibility (reprinted from Evans & Heller, 2003). The data on the right is $\delta^{18}O$ data from Shackleton et al. (1990) and the magnetic data from Xifeng is from Liu et al. (1988).

the production of reduced iron as waste product (Lovley et al., 1987). This correlation between increased magnetic susceptibility and soil horizons is called a positive correlation and is seen in the classical Chinese loess deposits. In other loess deposits, such as the deposits at Kurtak in southern Siberia (Chlachula et al., 1997) and loess deposits in Alaska (Beget at al., 1990), the magnetic susceptibility shows negative correlation. This is because such deposits follow a wind strength dependent magnetic susceptibility where the wind controls the amount of magnetic material brought into the

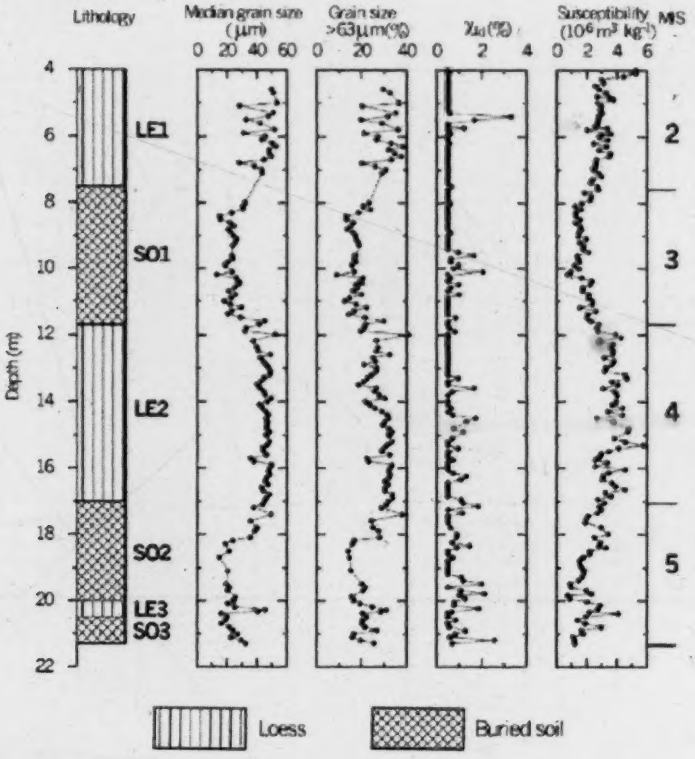

Figure 1.3 Kurtak section showing negative correlation where soil horizons with lower magnetic susceptibility and loess units with higher magnetic susceptibility (reprinted from Zhu et al., 2003).

susceptibility measurements while the larger magnetic minerals in the unaltered units are

depositional area and thereby the total magnetic susceptibility (Beget et al., 1990). This is because stronger winds are able to transport more magnetic material from the source area to the depositional site. In contrast, the weaker winds carry very little magnetic material to the depositional area (figure 1.3). In this case, there is less magnetic material to begin with, and this limits the capability of the bacteria to increase the susceptibility. However, in other Siberian loess/soil sequences magnetic susceptibility does not show either positive or negative correlation with soil horizons (Kravchinsky et al., 2007). This means that another parameter is required to be a proxy for pedogensis. The parameter that Kravchinsky et al. (2007) suggested to use is frequency dependence (FD) of magnetic susceptibility. Frequency dependence is a magnetic parameter that is determined by measuring both the low frequency magnetic susceptibility and the high frequency magnetic susceptibility, taking the difference and then dividing by the low frequency magnetic susceptibility. It is usually then multiplied by 100 and expressed as a percentage. The reason this parameter works as a proxy for pedogenesis is because, the magnetic material produced by bacteria during pedogenesis is microscopic and superparamagnetic magnetite which is detected by the high frequency magnetic not. Superparamagnetic magnetite is microscopic and therefore highly mobile physically. When the magnetic field is removed during testing of the magnetic susceptibility, the grains relax back to their original position before the field is reapplied. In this way they mimic the properties of true paramagnetic minerals. With a high frequency magnetic susceptibility test, however, the field is turned back on before the superparamagnetic magnetite has the opportunity to relax. This means that the altered soil units display

frequency dependence. These parameters are important tools in studying the climate changes in a continental setting.

The Holocene climate of the North Atlantic is strongly controlled by the mixing of waters between all the different ocean basins. This mixing is triggered by a mechanism called thermohaline circulation (Rahmstorf, 2006). Thermohaline circulation is the movement of ocean water based on both heat and variations in salinity. The influx of cold, low saline glacial water can strongly impact this circulation and thereby impacts the global ocean climate. The effect of this influx through the Holocene has been observed in the North Atlantic using isotopic data obtained from ice cores and from ice rafted debris (Bond et al., 1992). The effect on the ocean system has also been observed in the monsoons of the Indian Ocean (Gupta et al., 2005). Climate cyclicity through the Holocene has only been observed in marine or near marine settings and is strongly controlled by the influx of glacial input in the North Atlantic. A proposed trigger for this influx of glacial material is variations in solar energy (Bond et al., 2001). Periods of increased solar energy would increase the input of glacial material, while during periods of lower solar activity the influx of glacial material would decrease. The cycle of variability in solar energy over the Holocene is also known as insolation. The frequency of changes in ocean climate has been determined from data from the North Atlantic. The frequency varies from centennial scale to millennial scale. Periodicities of ~2500, ~1500, and ~900 yrs are generally the consensus for millennial scale cyclicity (Bond et al, 1992; Bianchi and McCave, 1999; Schulz and Paul, 2002). These periodicities are observed in the Greenland Ice Sheet Project Two (GISP2) data that has been studied by many

different researchers. Insolation with a 900 yr component has been proposed to be a potential driving force for the 900 yr cycle (Schulz and Paul, 2002). Glacial influx influenced by solar variability has been proposed to be cause of the 1500 yr cycles registered in the North Atlantic (Bond et al, 2001).

The site chosen for this study is located in the Selenga River valley of southern Siberia near Lake Baikal. There are a number of reasons why this site was chosen for study. The site contains a continuous Holocene loess/soil sequence which allows us to construct a detailed stratigraphic sequence. While most Holocene deposits that are studied for climate cyclicity are from marine or near marine settings, this site is a remote continental setting that is far from a marine setting. What this will provide is a record of Holocene climate that is as independent of ocean climate cycles as possible. As well, the site has provided samples for absolute dating, which, when combined with the stratigraphy of the site, allows for the determination of climate cyclicity in a region where marine influence on climate would be minimal or nonexistent. If the climate in the Selenga River valley shows climate cyclicity, which we expect it should due to the repetition of loess and soil horizons, then that cyclicity can be compared to that seen in marine records. If the periodicity of the climate change in the Selenga River valley correlates with periodicities from marine records, then Holocene climate change is truly global in nature. At the site a detailed description of the units was developed and samples were collected for this study. A complete description of the site is given in chapter 2. The samples collected included extensive samples for the magnetic experiments and several bulk samples for grain size

analysis. The sampling methodology is described in detail in chapter 3. The complete description of the units is given in chapter 4.

Once out of the field, the procedure was to use the detailed description and correlation between the trenches to build a complete depositional history. Radiocarbon dates that were obtained from a preliminary expedition in 2001 to the site could then be applied to the complete section and an age model could be developed. The other procedures performed included analyzing the samples for magnetic analysis in order to provide information on magnetic mineralogy and parameters. The bulk samples used for grain size analysis provide information on depositional setting as well as wind strength. The magnetic samples were tested for low frequency and high frequency magnetic susceptibility and this provided us with the frequency dependent magnetic susceptibility (FD) of each sample. The FD can then be used as a proxy for the relative extent of pedogenesis that has occurred. This is because as the amount of superparamagnetic material produced through bacterial activity increases, the high frequency magnetic susceptibility decreases. The result is a greater difference between low and high frequency susceptibility and therefore a higher FD. In addition, FD has recently been successfully used to characterize Mid- to Upper Pleistocene loess/soil sequences in western-central Siberia where magnetic susceptibility showed no correlation between magnetic susceptibility and loess/soil sequences (Kravchinsky et al., 2007). The samples were also tested using a high temperature scan and also for isothermal remnant magnetization (IRM) to determine magnetic mineralogy. The bulk grain size analysis allowed us to determine the sand, silt and clay fractions as well as the median grain size.

This provided us with a proxy for wind strength at the time of deposition as well as our model for the loess/soil formation. A detailed description of the testing procedure can be found in chapter 3 and the results of the analyses can be found in chapter 5. Once the data has been collected, the age model can then be applied to the data and any cyclicity present can be determined. Once the age model has been applied, a spectral analysis can be performed. After applying a spectral analysis to the North Atlantic data available, the periodicities from both the North Atlantic and the Burdukovo site can be compared. This spectral analysis will provide evidence of Holocene climate cyclicity. It is the aim of this research to show whether or not that Holocene climate cyclicity is global or not.

Chapter 2 Study Sites

Holocene records characterising climatic conditions are primarily glacial records, ocean cores, and loess deposits. Of these, glacial records and ocean cores are most commonly used. In southern Siberia a complete Holocene loess record, gives a climatic history for 10ky. The Burdukovo site has several advantages, such as being a continuous Holocene loess section, being mid-continental, and proximity to Lake Baikal. A continuous Holocene loess section means that it provides a continuous climatic record for the last 10ky. Being a mid-continental location means that oceanic effects on climate are minimised. The proximity to Lake Baikal means that the record can be easily compared to Holocene data from drilling cores taken from the lake.

The area that was sampled for Holocene deposits was a terrace in the Selenga River valley, east of Lake Baikal. The site is located at 52.1°N and 107.5°E and at an elevation of approximately 500m, just outside of the village of Burdukovo. The terrace that was sampled is on the northern shore of the Selenga River and has southwest exposure. Four trenches were dug into the terrace to expose sediments that were more cohesive and would allow for sampling of oriented samples. Of the four trenches, only three were sampled; trench 1, trench 3, and trench 4. The most prominent buried soil was traced along the terrace and formed a series of paleo-depressions and plateaus. Trench 1 was located near the base of a paleo-depression and was 4.05m from the top of the terrace to the bottom of the trench (figure 2.2). Trench 3 was at a plateau and exposed 3.45m of sediment (figure 2.2). Trenches 2 and 4 were both located in the transition zone of a paleo-depression. Trench 4 had undergone less post depositional disturbance and was

selected for sampling. Trench 4 was 4.40m from the top of the terrace to the bottom of the trench and contained the contact between the Holocene deposits and earlier alluvial sand and gravel (figure 2.3).

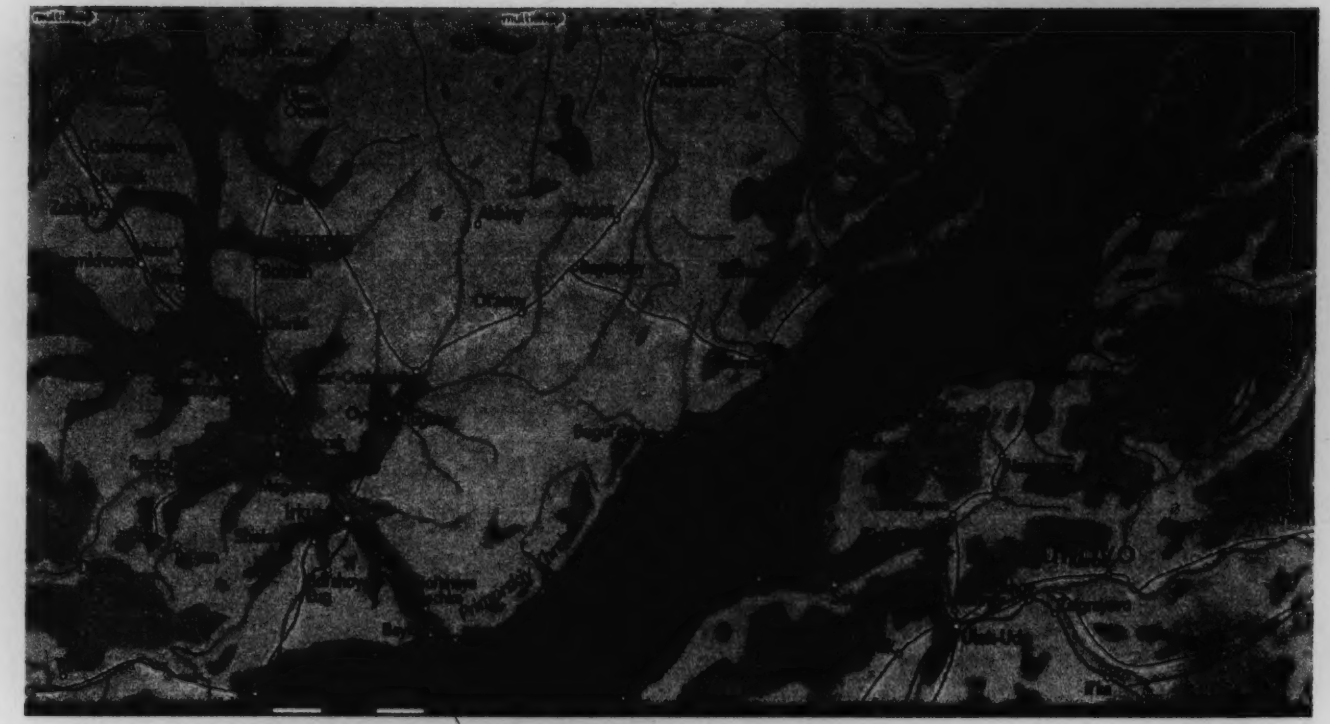

Figure 2.1 Location of Burdukovo study site (map adapted from Collins Bartholomew Ltd., 2003).

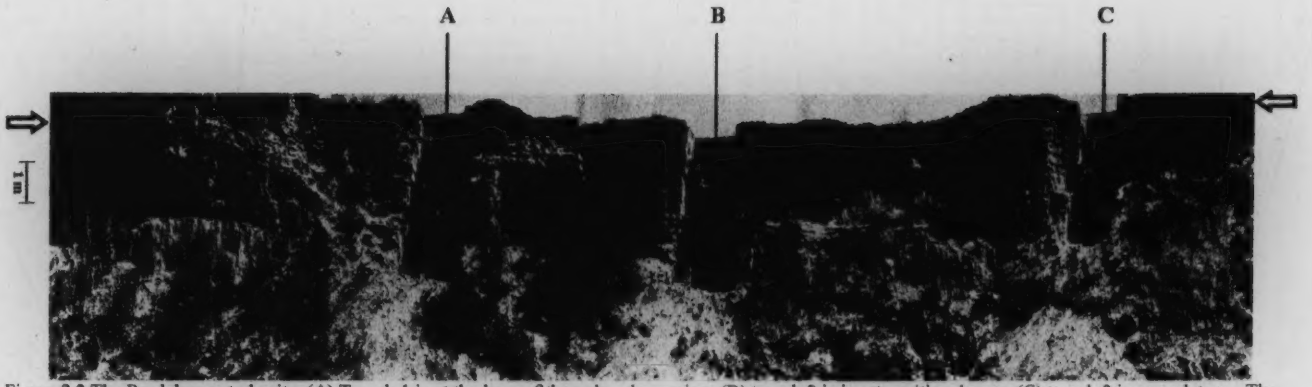

Figure 2.2 The Burdukovo study site. (A) Trench 1 is at the base of the paleo-depression, (B) trench 2 is in a transitional zone, (C) trench 3 is on a plateau. The arrows on either side of the figure are indicating the top of unit 11, also referred to as the main buried soil. As the most well developed buried soil, it was used as the datum for correlation of the units between the individual trenches.

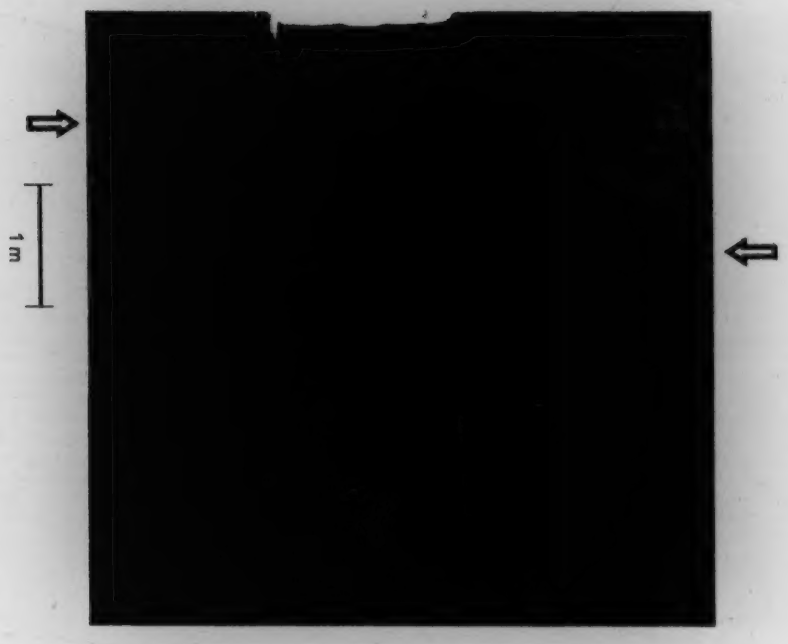

Figure 2.3 Trench 4 at the Burdukovo site. The arrows indicate unit 11, the datum unit used for correlation.

Chapter 3 Methodology

Sampling Method

Sampling at the Burdukovo site included collecting both oriented and unoriented samples for magnetic study. Oriented samples were taken at 5cm intervals with unoriented samples taken between each oriented sample. Each oriented sample was collected by inserting 2.1cmx2.1cmx5cm metal sheath (figure 3.1) into the exposed sediments. The sample was then extracted from the sheath and preserved in an $8cm^3$ plastic cube. Because of the dimensions of the samples, a 3cm space between each sample remained, which was then collected as bulk samples. This provided a continuous sample profile for testing of the magnetic susceptibility. The primary difficulty encountered during sampling was the exposed sediments dried and lost cohesion quickly under sunny and hot conditions. This rendered some of the samples less than ideal for measuring such parameters as anisotropy but did not affect magnetic susceptibility measurements. Sampling also included collecting approximately 100g from each loess and buried soil unit for geochemical and grain size analyses. Other samples also collected included micromorphological samples for studying microstructures, OSL samples for potential age dating, and mollusc samples for potential age dating.

Testing Methods and Equipment

The samples brought back for magnetic study were tested for mass specific magnetic susceptibility in order to determine relative amount of pedogenesis. Mass specific susceptibility was measured rather than volume specific susceptibility because the density of the samples varied while the volume remained constant and all that is required for mass specific susceptibility is careful weighing the samples prior to measurement.

Testing of the mass specific magnetic susceptibility was carried out using a Bartington MS2 susceptibility meter (figure 3.2). The oriented samples were weighed and then tested for both low frequency susceptibility and high frequency susceptibility. The low frequency magnetic susceptibility was measured three times and the average was calculated. After measuring the low frequency magnetic susceptibility of ten samples, those same ten samples were then measured for the high frequency magnetic susceptibility three times and the average was calculated. The samples were measured three times to account for any variability in the surrounding magnetic field. The high frequency magnetic susceptibility was measured after every ten samples so that both the low and high frequency magnetic susceptibilities were measured at the same approximate time and therefore the surrounding magnetic field would not have changed significantly. The frequencies that were used were 0.465kHz for the low frequency and 4.65kHz for the high frequency. This resulted in a ratio of low frequency to high frequency of 1:10. Once both the low and the high frequency susceptibility are determined the frequency dependent susceptibility percentage (FD) of the sample can be determined. The FD is the difference between high and low frequency susceptibility divided by the low frequency susceptibility.

$$X_{FD}\% = 100 \times ((X_{LF} - X_{HF}) / X_{LF})$$

Where $X_{FD}\%$ represents the frequency dependence, X_{LF} is the low frequency magnetic susceptibility, and X_{HF} is the high frequency magnetic susceptibility.

The unoriented samples required more preparation. They were packed into an $8cm^3$ sample box, compacted, and then weighed before testing. In order to insure maximum

Chapter 3 Methodology

Sampling Method

Sampling at the Burdukovo site included collecting both oriented and unoriented samples for magnetic study. Oriented samples were taken at 5cm intervals with unoriented samples taken between each oriented sample. Each oriented sample was collected by inserting 2.1cmx2.1cmx5cm metal sheath (figure 3.1) into the exposed sediments. The sample was then extracted from the sheath and preserved in an $8cm^3$ plastic cube. Because of the dimensions of the samples, a 3cm space between each sample remained, which was then collected as bulk samples. This provided a continuous sample profile for testing of the magnetic susceptibility. The primary difficulty encountered during sampling was the exposed sediments dried and lost cohesion quickly under sunny and hot conditions. This rendered some of the samples less than ideal for measuring such parameters as anisotropy but did not affect magnetic susceptibility measurements. Sampling also included collecting approximately 100g from each loess and buried soil unit for geochemical and grain size analyses. Other samples also collected included micromorphological samples for studying microstructures, OSL samples for potential age dating, and mollusc samples for potential age dating.

Testing Methods and Equipment

The samples brought back for magnetic study were tested for mass specific magnetic susceptibility in order to determine relative amount of pedogenesis. Mass specific susceptibility was measured rather than volume specific susceptibility because the density of the samples varied while the volume remained constant and all that is required for mass specific susceptibility is careful weighing the samples prior to measurement.

2006). The Sedigraph 5100 also measured the median grain size, which will also show a dependency on relative wind strength, and may prove more useful for this study.

Figure 3.2 Bartington MS2 dual frequency magnetic susceptibility meter

Figure 3.3 Micrometrics SediGraph 5100

Chapter 4 Stratigraphy and Sedimentology

This chapter presents field observations and descriptions and uses them to construct a stratigraphic sequence for the Holocene deposits of the Burdukovo. The correlation of the stratigraphy at the Burdukovo site is important due to age dating having been done for trench four only. The correlation of the Burdukovo site was accomplished using the unit descriptions as well as physical features. The most strongly developed buried soil, subunit 11 in each trench, was used as the datum for correlation as it could be traced along the terrace and could be easily identified in each trench. The soil and loess units were differentiated by a number of features. The primary features included colour, the existence of pedogenic structure, and evidence of root systems. Other features are described in the individual description of the units. Also included in the descriptions is the presence of mezzofaunal traces, as well as krotovinas. These are animal trace structures, mezzofauna are medium size animals that would include insects and worms and krotovinas are burrows from larger animals such as moles or gophers. The dimensions of these trace structures are given in the unit descriptions in which they are found.

The Holocene deposits of the Burdukovo site are located on the northern terrace of the Selenga River valley, approximately 70 km east of Lake Baikal. The uppermost sediments at the site are eolian in origin while the bottom sedimentary layers are interpreted as being fluvial in origin. Trench 1 is located near the base of a paleo-depression (figure 2.1) that has been interpreted as a former tributary channel. Trench 3

is located at a plateau separating paleo-depressions (figure 2.1). Trench 4 is located at a transitional point between a paleo-depression and the plateau (figure 2.2).

Burdukovo Section: Trench 1

Trench 1 (referred to as BD1) contains seven primary units extending from the surface to a depth of 4.05 metres. Each unit contains various subunits and can be seen in further detail in figure 4.1.

BD1-16: 0 – 119 cm

The uppermost unit, BD1-16 contains six subunits and is defined by the presence of living root systems. BD1-16a is the surface soil containing abundant living roots and having a weak to very weak granular structure. The thickness of the subunit is 3 cm and it has a planar, transitional lower boundary. Subunit BD1-16b is a loamy sand containing common living roots and having weak angular blocky structure. The subunit extended from 3 cm to 17 cm and the lower boundary clear and planar with common mezzofaunal traces penetrating into subunit BD1-16c. Subunit BD1-16c is loamy sand with a massive texture containing common living roots. The subunit also contains krotovinas that are up to 5 cm in diameter and filled with material from BD1-16b and have diffuse boundaries. Subunit BD1-16c extends from 17 cm to 24 cm and the lower boundary is wavy and diffuse. Subunit BD1-16d is loamy sand that has traces of a former granular structure and contains common living roots. The subunit has a consistent thickness and a diffuse, wavy lower boundary that is disturbed with mezzofaunal traces. Subunit BD1-16e is sand to loamy sand. It is a stratified unit with alternating juvenile buried soils and unaltered eolian sand layers. The juvenile buried soils are laminated but contain no

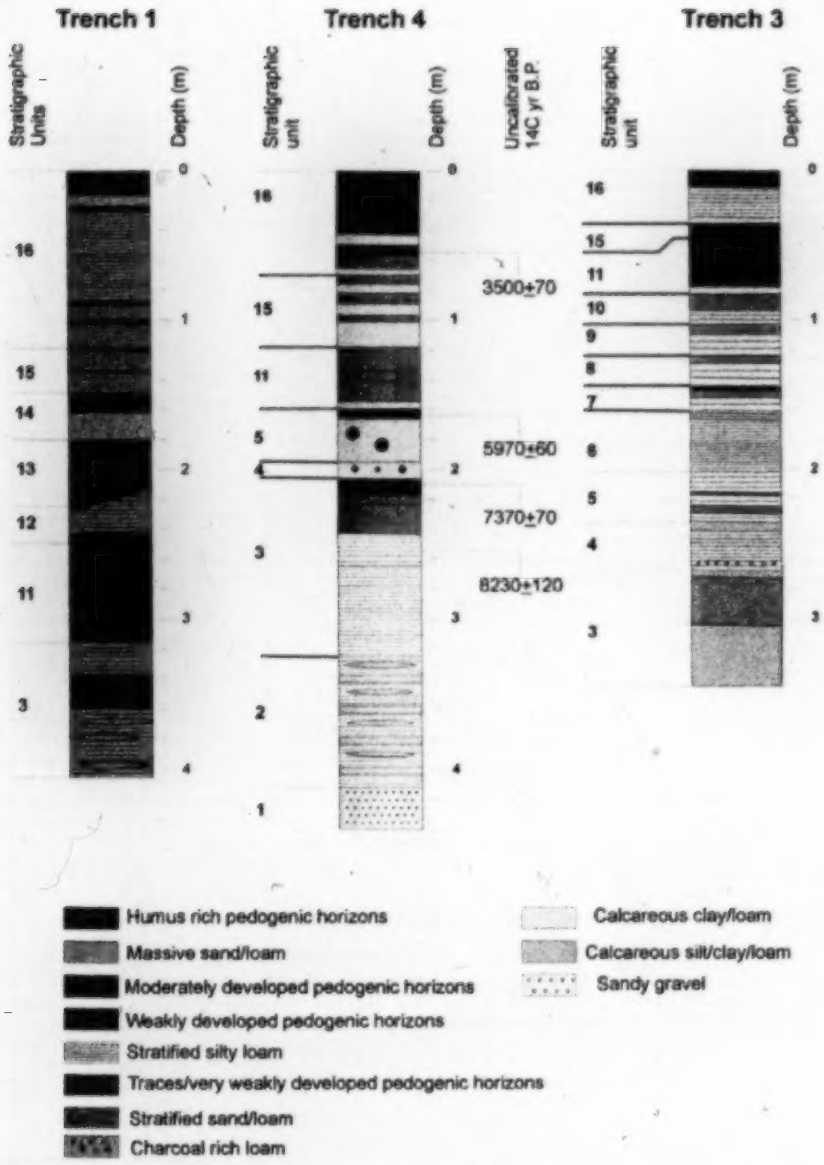

Figure 4.1 Stratigraphic sections for trenches 1, 3, and 4 at the Burdukovo site.

pedogenic structures and vary in thickness from 3 to 8 cm. The eolian sand layers vary in thickness from 4 to 12 cm. The unit contains few living roots and has been disturbed by bird burrows. The unit extends from 28 cm to a depth of 87 cm and has a clear lower boundary. Subunit BD1-16f is similar to the previous subunit in that contains alternating buried soils and eolian sand layers. The buried soils in BD1-16f however, are effervescent and are very weak sub-angular blocky with a weak laminated texture. They are porous and are of consistent thickness and are extend from 87 to 91 cm and from 99 to 103 cm with clear upper and lower boundaries. The eolian sand layers have few pores, few charcoal fragments (up to 2 mm in diameter) and do not effervesce. They extend from 91 to 99 cm and from 103 to 119 cm. They are laminated and display crossbedding at the base of the layer. The lower boundary is sharp, irregular and disturbed with mezzofaunal traces.

BD1-15: 119 to 148 cm

Unit BD1-15 consists of four subunits and contains no living roots. Subunit BD1-15a is loamy sand that is consistent in thickness and heavily disturbed by mezzofaunal traces. The lower boundary is slightly wavy and clear at a depth of 121 cm. Subunit BD1-15b is stratified sand. It is slightly porous and has common Fe mottling (1 to 3 mm in diameter). The unit extends from 121 to 133 cm. The lower boundary is sharp, planar, and disturbed by mezzofaunal traces. Subunit BD1-15c is also loamy sand that is consistent in thickness and heavily disturbed by mezzofaunal traces. The lower boundary is slightly wavy and clear. The unit extends from 133 to 136 cm. Subunit BD1-15d is stratified loamy sand that contains common Fe mottling (up to 5 mm in diameter) and few charcoal fragments (up to 3 mm in diameter). The unit extends from 136 to 148 cm

and the lower boundary is slightly wavy, sharp and slightly disturbed with mezzofaunal traces.

BD1-14: 148 to 180 cm

Unit BD1-14 is divided into three subunits. Subunit BD1-14a is loamy sand and contains few single pebbles. There are traces of granular to sub-angular blocky structure. The subunit extends from 148 to 155 cm and has a transitional lower boundary. Subunit BD1-14b is sand and contains a single, irregular crack. Mezzofaunal traces are common and there are 5 cm wide pockets at the bottom of the unit that penetrate to 180 cm depth. The subunit extends from 155 to 162 cm and has a clear lower boundary. Subunit BD1-14c is massive sand, has a few mezzofaunal traces and a few Fe nodules (up to 2 mm in diameter). There are also contains very faint traces of pedogenic structure. The subunit extends from 162 to 180 cm and has a clear, planar lower boundary.

BD1-13: 180 to 225 (210) cm

Unit BD1-13 is separated into two subunits. BD1-13a is fine sand with a sub-angular blocky structure. It extends from 180 to 188 cm and has few mezzofaunal traces along its transitional lower boundary. Subunit BD1-13b is fine to medium sand and has traces of pedogenic structure. The lower boundary of the unit follows the paleo-depression. On the right hand side of the trench the bottom of the unit is at 210 cm, and on the left side of the trench the bottom of the trench is at a depth of 225 cm.

BD1-12: 225 (210) to 250 (235) cm

Unit BD1-12 is sand and is divided into four subunits. Subunit BD1-12a contains abundant mezzofaunal traces and is slightly effervescent at the top of the unit due to precipitation of post-depositional carbonates. The carbonates are only present at the top

of the unit at the bottom of the paleo-depression (i.e. they are not present where unit BD1-12 rises towards the plateau). The subunit has a uniform thickness of 4 cm and a clear lower boundary that is at a depth of 2.14 cm on the right side of the trench and a depth of 229 cm on the left side of the trench. Subunit BD1-12b is crossbedded sand with weakly pronounced stratification. In the upper portion of the subunit, the layers follow the upper boundary, while at the bottom they are horizontal and follow the lower boundary. The subunit contains a few larger charcoal fragments (up to 5 mm × 10 mm) and common massive sand lenses (4 cm × 20 cm) that are enriched with very small charcoal pieces (less than 1 mm in diameter). The lower boundary is clear planar, and is disturbed by mezzofaunal traces. The lower boundary is at a depth of 242 cm on the left side of the trench while on the left side the lower boundary is at a depth of 235 cm and sits on unit BD1-11. Subunit BD1-12c is loamy sand and contains few carbonates and Fe mottling (up to 5 mm in diameter) along the upper boundary. The subunit is very porous, disturbed by many mezzofaunal traces (up to 3 mm in diameter), and has weak sub-angular structure. The lower boundary is transitional, planar, and strongly disturbed by mezzofaunal traces. On the left side of the trench the lower boundary is at a depth of 246 cm. Subunit BD1-12d is crossbedded sand containing charcoal fragments (up to 2 mm in diameter). When wet, common mezzofaunal traces are visible. The maximum thickness at the base of the paleo depression is 9 cm (1 m left of trench BD1). The lower boundary is irregular, slightly wavy, and slopes towards the centre of the paleo-depression at an angle of approximately 1°. The boundary is also strongly disturbed by mezzofaunal traces and is at a depth of 250 cm on the left portion of the trench.

BD1-11: 250 (235) to 320 (310) cm

Unit BD1-11 is the main buried soil and is not divided into any subunits. The unit contains lenses of dark, humus rich material. There are nine lenses that are generally 40 to 60 cm wide approximately 10 cm thick, concave upward, and they overprint older lenses. The humus enrichment of the lenses decreases with depth and porous sub-angular blocky structure is present in all lenses but two, from 268 to 276 cm and 287 to 296 cm. The lower boundary is irregular and clear by effervescence. Unit 11 sits directly over unit BD1-5. Units 10 through 4 are not present in trench 1. They have been incorporated into unit11 in the paleo-depression during deposition.

BD1-3: 320 (310) to 405 cm (bottom of trench 1)

Unit BD1-3 is stratified alluvium and is divided into three subunits. Subunit BD1-3a is silty loam with white calcareous spots. The subunit is moderately stratified, porous, and effervescent. It also contains few mezzofaunal traces and traces of sub-angular blocky structure. The subunit is colluvial, having been redeposited. The lower boundary is clear and irregular ranging from 322 to 337 cm in depth. Subunit BD1-3b is silty loam that is very porous with carbonates in the pores. It also contains a few shells few mezzofaunal traces, weak pedogenic structure, and is weakly stratified. It has a transitional lower boundary at 360 cm depth. Subunit BD1-3c is stratified silty loam that is very porous, very calcareous, and contains coarse sand lenses and krotovinas. The subunit contains few shells and has a platy texture. The sand lenses are medium to coarse grained sand and a few pebbles (up to 4.5 cm long axis diameter). They are discontinuous and 0.5 to 5 cm thick. The krotovinas are approximately 5 cm in diameter and filled with material from unit BD1-11, and subunits BD1-3a and BD1-3b. The lower boundary of the unit

was not exposed at the bottom of trench, however the upper level of the fluvial sand and gravel could be observed at a depth of 515 cm.

Burdukovo Section: Trench 3

Trench 3 (referred to as BD-3) contains 11 units extending from the surface to a depth of 3.45 metres. The units are divided into subunits and can be seen in further detail in figure 4.3.

BD3-16: 0 – 35 cm

Unit BD3-16 consists of four subunits and contains the modern soil with abundant living root systems. Subunit BD3-16a is the uppermost topsoil and contains abundant living roots. The subunit is 3 cm thick and has a planar lower boundary. Subunit BD3-16b is loamy sand and contains many living roots. It has a weak to fine sub-angular blocky structure. The subunit extends from 3 cm to 12 cm and has a transitional lower boundary. Subunit BD3-16c is a laminated unit, with loamy sand layers and fine sand layers. There are three loamy sand layers separated by two fine sand layers. The layers are 5 cm to 7 cm thick, sub-horizontal and have clear boundaries. The entire subunit extends from 12 cm to 32 cm and has a clear planar lower boundary. Subunit BD3-16d is medium sand containing living roots. It is disturbed mezzofaunal traces and root traces. There is some Fe mottling among living roots. The subunit is 3cm thick with the lower boundary at 35 cm depth, however mezzofaunal disturbance of the lower boundary allows for material from the subunit to extend to 36 cm depth.

BD3-15: 35 – 46 cm

Unit BD3-15 is a buried soil and contains two subunits. Subunit BD3-15a is silty sand with weak sub-angular blocky structure. The subunit extends from 35 cm to 40 cm and

has a clear planar lower boundary. Subunit BD3-15b is loamy sand with weak sub-angular blocky structure. It is slightly porous and contains a few living roots. The subunit is 6 cm thick with a wavy lower boundary at 46 cm that is disturbed with mezzofaunal traces.

BD3-11: 46 – 83 cm

Unit BD3-11 is the main buried soil and is divided into three subunits. Subunit BD3-11a is sandy loam with moderate sub-angular blocky structure. The subunit contains few living roots and a few mezzofaunal traces. The subunit extends from 46 cm to 58 cm and has a transitional lower boundary. Subunit BD3-11b is sandy loam with moderate sub-angular blocky, similar to subunit BD3-11a but with a higher sand content. The subunit extends from 58 cm to 64 cm and has a transitional lower boundary. Subunit BD3-11c is sandy loam with a stronger moderate sub-angular blocky structure than the previous subunits. The subunit extends from 64 cm to 78 cm and has a transitional, planar lower boundary. Subunit BD3-11d is fine sand that is weakly stratified. The unit is non-calcareous except for common carbonate deposits around root traces. The subunit extends from 78 cm to 83 cm and has a transitional, planar lower boundary that is disturbed with mezzofaunal traces.

BD3-10: 83 – 103 cm

Unit BD3-10 contains a buried soil and is divided two subunits. Subunit BD3-10a is the buried soil and is loamy sand with weak traces of sub-angular structure. The subunit is non-calcareous but contains carbonates along root traces. The lower boundary is irregular and disturbed by mezzofaunal traces causing the lower boundary to vary from 93 cm to 95 cm. Subunit BD3-10b is weakly stratified loamy sand and fine sand. The

subunit contains few carbonates along pores, many weak Fe mottling and weak gley mottling. Gley mottling is a colour pattern that is the result of the unit being waterlogged and anaerobic, which also results in the reduction of iron in the unit (Pansu and Gautheyrou, 2006). The thickness of the unit is 8 cm to 10 cm with an irregular lower boundary at 103 cm depth that is disturbed with mezzofaunal traces.

BD3-9: 103 – 124 cm

Unit BD3-9 is a buried soil with two subunits. Subunit BD3-9a is fine sand with very weak sub-angular blocky structure. The subunit is weakly porous with few carbonates along the pores and mezzofaunal traces are common throughout the subunit. The subunit extends from 103 cm to 110 cm and has a clear, planar lower boundary that is disturbed with mezzofaunal traces. Subunit BD3-9b is fine sand that is weakly stratified. The subunit contains mezzofaunal traces that are sub-vertical and up to 7 mm in diameter. The subunit also contains few weak gley mottling. The subunit extends from 110 cm to 124 cm and has a clear, planar lower boundary that is disturbed with mezzofaunal traces.

BD3-8: 124 – 144 cm

Unit BD3-8 has the same characteristics as unit BD3-9. It contains a buried soil and is divided into two subunits. Subunit BD3-9a is the buried soil and is fine sand with very weak sub-angular blocky pedogenic structure. The subunit is weakly porous with some carbonates along the pores and common mezzofaunal traces. The lower boundary is at a depth of 129 cm and is clear, planar, and disturbed with mezzofaunal traces. Subunit BD3-8b is fine sand that is weakly stratified. The subunit contains sub-vertical mezzofaunal traces and few weak gley mottling. The lower boundary is at a depth of 144 cm and is clear, planar, and disturbed with mezzofaunal traces.

BD3-7: 144 – 161 cm

Unit BD3-7 contains a buried soil and is divided into three subunits, with subunits BD3-7a and BD3-7b making up the buried soil. Subunit BD3-7a is sandy loam with weak sub-angular blocky to granular structure and is very porous. The subunit extends from 144 cm to 147 cm and has a clear, planar lower boundary that is disturbed with mezzofaunal traces. Subunit BD3-7b is loamy sand with granular to very weak sub-angular blocky pedogenic structure and contains many mezzofaunal traces. The lower boundary is at a depth of 152 cm, is irregular, planar, and disturbed by mezzofaunal traces and pockets that are 5 cm wide and 5 cm deep. Subunit BD3-7c is fine sand that is weakly stratified. The stratified layers that are darker in colour have traces of pedogenic structure. The subunit extends from 152 cm to 161 cm and has a transitional, wavy lower boundary.

BD3-6: 161 – 202 cm

Unit BD3-6 is a 41 cm thick stratified sand unit. The only feature of the unit is the alternating layers of laminated fine sands and massive coarse sands. The lower boundary is at a depth of 202 cm and is sharp and wavy.

BD3-5: 202 – 236 cm

Unit BD3-5 contains five subunits which alternate from fine sand to sandy loam. Subunit BD3-5a is laminated fine sand. The subunit is disturbed with mezzofaunal traces and contains charcoal fragments that are up to 1 cm in diameter. The lower boundary is at a depth of 216 cm, is sharp, planar, and slightly disturbed by mezzofaunal traces. Subunit BD3-5b is sandy loam with very weak granular structure. The subunit is porous with common carbonates along the pores but the rest of the subunit is non-calcareous. There are many mezzofaunal traces as well as a unique krotovina that is 9 cm in diameter

penetrating through subunit BD3-5c into the top of subunit BD3-5d and is very well preserved. The subunit extends from 216 cm to 218 cm and has an irregular lower boundary that is very strongly disturbed with mezzofaunal traces. Subunit BD3-5c is fine sand with weak crossbedded lamination. The subunit contains few mezzofaunal traces and the krotovina that penetrates from subunit BD3-5b. The lower boundary is at a depth of 225 cm, is irregular, sub-horizontal, and disturbed with pockets and mezzofaunal traces. Subunit BD3-5d is loamy sand with very weak granular to fine sub-angular blocky pedogenic structure. The subunit is strongly disturbed with mezzofaunal traces and contains many carbonates along pores. The subunit extends from225 cm to 230 cm and has a clear wavy lower boundary that is disturbed with mezzofaunal traces. Subunit BD3-5e is fine sand that is weakly stratified. The subunit contains few mezzofaunal traces and a 5 mm thick carbonate rich band at the base of the subunit. There is variable effervescence in the rest of the subunit. The subunit extends from 230 cm to 236 cm and has a sharp wavy lower boundary.

BD3-4: 236 – 268 cm

Unit BD3-4 is divided into four subunits. Subunit BD3-4a is loam with weak sub-angular blocky divided into granular structure. The subunit contains common small shells and many mezzofaunal traces. The subunit extends from 236 cm to 242 cm and has a transitional lower boundary. Subunit BD3-4b is laminated silty loam and has no pedogenic structures. The subunit contains a few pebbles that are up to 4 cm along the long axis, common mezzofaunal traces, charcoal fragments and many shells. The subunit is slightly porous with carbonates along the pores in the lower portion. The lower boundary is clear at a depth of 262 cm. Subunit BD3-4c is loam with very weak sub-

angular blocky structure. The subunit is lens like with a maximum thickness of 7 cm and is slightly porous. It is strongly enriched with large charcoal pieces that are up to 1.5 cm wide and 7 cm long. The charcoal covers approximately 30% of the surface area. The lower boundary is sharp and irregular at a depth of 265 cm. Subunit BD3-4d is sandy loam that is weakly stratified. The subunit is discontinuous, or lens like, and contains carbonates that follow the stratification. The lower boundary is at a depth of 268 cm and is sub-horizontal, irregular and clear to sharp.

BD3-3: 268 – 345 cm (bottom of trench 3)

Unit BD3-3 is alluvium that is divided into three subunits and contains a buried soil near the top of the unit. Subunit BD3-3a is silty to clayey loam that is very porous with carbonates along the pores. The subunit extends from 268 cm to 273 cm and has a clear planar lower boundary. Subunit BD3-3b is the buried soil and is silty loam with very weak granular to sub-angular blocky pedogenic structure. The subunit contains common Fe/Mn nodules that range from 1 mm to 7 mm in diameter, common shells that are up to 4 mm in diameter and few single pebbles that are up to 1 cm along the long axis. The subunit is porous and has common carbonate coating along the pores. The lower boundary is clear, irregular and varies from 290 cm to 305 cm depth. Subunit BD3-3c is weakly stratified silty loam. The subunit is porous with calcareous deposits occurring mostly along the pores. It also contains many Fe/Mn nodules that are up to 2 mm in diameter and common shells. The subunit extends to the bottom of trench 3 at a depth of 345 cm.

Burdukovo Section: Trench 4

Trench 4 (referred to as BD-4) is divided into eight units and extends from the surface to

a depth of 4.40 metres. A more detailed section can be seen in figure 4.3.

BD4-16: 0 – 70 cm

Unit BD4-16 contains nine subunits and includes the modern soil and contains living root systems. Subunit BD4-16a is the top 3 cm of the unit, contains abundant living roots and has a planar lower boundary. Subunit BD4-16b is loamy sand that contains many living roots and has a sub-angular blocky to granular pedogenic structure. The subunit has a planar lower boundary at 10 cm depth. Subunit BD4-16c is loamy sand that contains many living roots and has a sub-angular blocky pedogenic structure that has weakly granular substructure. The lower boundary is clear, wavy, and is at a depth of 36 cm. Subunit BD4-16d is loamy sand that has a weak sub-angular blocky pedogenic structure. The subunit has a transitional lower boundary at 43 cm depth that is disturbed with mezzofaunal traces. Subunit BD4-16e is loamy sand to fine sand and contains few living roots. The lower boundary is clear, slightly wavy, and disturbed with mezzofauna. The depth of the lower boundary varies from 48 cm to 51 cm. Subunit BD4-16f is fine sand and has weak sub-angular blocky pedogenic structure. The lower boundary is diffuse at a depth of 57 cm. Subunit BD4-16g is fine sand and has very weak sub-angular blocky pedogenic structure. The subunit also contains rare small pebbles that had a long axis up to 7 cm. The lower boundary is clear, planar, and slightly disturbed with mezzofauna. The lower boundary of the subunit is at a depth of 63 cm. Subunit BD4-16h is fine sand and has very weak sub-angular blocky pedogenic structure. The lower boundary is clear but irregular, sub-horizontal, and disturbed with mezzofauna. The depth of the lower boundary is 66 cm. Subunit BD4-16i is massive fine sand that contains few living roots and few mezzofaunal traces. The colour of the subunit darkens towards the bottom. The

lower boundary is very slightly wavy, almost to the point of being planar. The lower boundary is strongly disturbed with mezzofauna and is at a depth of 70 cm.

BD4-15: 70 – 118 cm

Unit BD4-15 is a sandy unit that is divided into six subunits and has a consistent thickness of 48 cm within the trench. Subunit BD4-15a is fine sand to loamy sand and contains many mezzofaunal traces. The subunit has very weak sub-angular blocky pedogenic structure with traces of granular structure. The subunit has a clear lower boundary at 76 cm depth and is disturbed with mezzofauna. Subunit BD4-15b is fine sand that contains many mezzofaunal traces and a few charcoal fragments. The charcoal fragments are usually less than 1 mm but there were rare fragments that measured up to 15 mm in length and 5 mm in width. The lower boundary is clear, wavy, and disturbed with mezzofauna. The depth of the lower boundary varies from 79 cm to 82 cm. Subunit BD4-15c is fine sand with traces of sub-angular blocky structure. The subunit is disturbed with disturbed with mezzofauna and krotovinas. The krotovinas are approximately 6 cm in diameter and their boundaries are moderately disturbed with mezzofauna. The lower boundary varies from 82 cm to 89 cm depth and is clear, irregular, and strongly disturbed with mezzofauna. Subunit BD4-15d is massive medium sand with common mezzofaunal traces and few krotovinas in the upper portion. The lower boundary is planar and disturbed with mezzofauna on the left side of the trench. The lower boundary is intersected by the sloped upper surface of unit BD4-11 on the left side of the trench. The lower boundary of the subunit is at a depth of 97 cm on the right side of the trench (all further measurements were taken on the right side of the trench). Subunit BD4-15e is loamy sand with traces of granular pedogenic structure. The subunit

contains many traces of mezzofauna and there are a few post-pedogenic carbonates present along the sub-vertical pores. The lower boundary is at a depth of 101 cm, slightly wavy and disturbed with mezzofauna. Subunit BD4-15f is fine sand and has no visible structure. The lower boundary of the subunit is at a depth of 118 cm, is clear and planar.

BD4-11: 118 – 159 cm

Unit BD4-11 is the main buried soil and is divided into four subunits. The upper boundary of the unit is at a depth of 94 cm on the left side of the trench and at a depth of 118 cm on the right side of the trench. The upper boundary slopes at 18 cm/m from left to right. Subunit BD4-11a is loamy sand and has very weak sub-angular blocky pedogenic structure with traces of granular structure. There are a few carbonates along the sub-vertical pores the cross the upper boundary while the rest of the subunit is non-calcareous. The subunit is porous and contains many mezzofaunal traces. The lower boundary is transitional and follows the upper boundary to a depth of 134 cm. Subunit BD4-11b is loamy sand that has traces of sub-angular blocky and granular pedogenic structures. It is slightly porous with many carbonates along the pores. The lower boundary is at a depth of 141 cm on the right side of the trench, is transitional and follows the upper boundary. Subunit BD4-11c is loamy sand to fine sand with traces of sub-angular blocky and granular structure. The subunit contains few carbonates along pores and is strongly disturbed with mezzofauna. The lower boundary is irregular and disturbed with mezzofauna. It generally follows the upper boundary and is at a depth of 154 cm on the right side of the trench. Subunit BD4-11d is fine sand that is massive with few mezzofaunal traces and very rare carbonates along pores. There are cracks present that start at the upper boundary of the subunit and penetrate to a depth of 190 cm. The

interval between cracks is approximately 40 cm, they are 2 cm wide at the top and they are filled with material from subunit BD4-11c. The lower boundary is irregular and disturbed with mezzofauna and krotovinas. The boundary slopes 10 cm/m from left to right to a depth of 159 cm on the right side of the trench.

BD4-5: 159 – 195 cm

Unit BD4-5 is a sandy unit with two subunits. Subunit BD4-5a is sandy loam that has a weak sub-angular blocky structure with traces of strong granular structure. The subunit is porous contains abundant traces of mezzofauna, and few Fe mottling. The lower boundary is at a depth of 166 cm, is irregular, and is generally parallel to the upper boundary. Subunit BD4-5b is massive fine sand that contains ferric deposits and carbonates along sub-vertical root traces. The subunit also contains thin cracks penetrating from unit BD4-11 and common krotovinas. The krotovinas are 8 to 9 cm in diameter and show evidence of multiple usage. The boundaries of the krotovinas are disturbed with mezzofauna and they penetrate into units BD4-4 and BD4-3. The lower boundary is strongly disturbed by krotovinas, slightly wavy, and sharp by effervescence. The lower boundary slopes 2 cm/m from left to right to a depth of 195 cm on the right side of the trench.

BD4-4: 195 – 206 cm

Unit BD4-4 consists of two subunits. Subunit BD4-4a is loamy sand that shows traces of pedogenic structure and disturbed by krotovinas. The subunit is very porous with carbonate mottling along the pores and is therefore strongly effervescent. The lower boundary follows the upper boundary and is at a depth of 201 cm. Subunit BD4-4b is clayey loam with strong, fine sub-angular blocky structure. The subunit is disturbed with

krotovinas, is porous and has strong effervescence. There are Fe coatings on some aggregates and platy texture is visible on the dry wall. The lower boundary is sub-horizontal and slightly wavy at a depth of 206 cm.

BD4-3: 206 – 325 cm

Unit BD4-3 is silty alluvium and is divided into six subunits. The entire unit is calcareous and has a buried soil at the top of the unit. Sub unit BD4-3a is silty loam with weak granular structure. The subunit is porous, disturbed with mezzofauna, and is interrupted with krotovinas from unit BD4-5. The subunit also contains common charcoal pieces (up to 5mm X 5mm in size) and many small shells. The lower boundary is irregular at 209cm and contains cracks that are ~10cm wide, 10cm to 15cm apart, and penetrate to a depth of 220cm. Subunit BD4-3b is silty loam with very calcareous sub-angular blocky structure. The subunit has very weak platy texture, is strongly disturbed with mezzofauna, and contains carbonates along pores and the surfaces of aggregates. The lower boundary is wavy and irregular at a depth of 217cm. Subunit BD4-3c is silty loam with traces of pedogenic structure. The subunit is calcareous with platy texture and contains many mezzofauna traces. The lower boundary is irregular at a depth of 223cm. Subunit BD4-3d is silty loam with weak traces of pedogenic structure. The subunit is calcareous, porous, and has weak platy texture. The subunit also contains rare pebbles (up to 10mm along the long axis) and krotovinas from unit BD4-5 that penetrate to a depth of 260cm. The lower boundary is irregular with cracks similar to subunit BD4-3a. The bottom of the subunit is at a depth of 243cm. Subunit BD4-3e is weakly stratified silty loam and is disturbed by krotovinas and cracks from previous subunit. The lower boundary is slightly wavy at a depth of 262cm. Subunit BD4-3f is weakly stratified silty

loam with platy texture. The subunit is calcareous, contains shells, weak Fe mottling, and common Fe/Mn nodules (up to 2mm in diameter). The stratified layers are wavy and are enriched with carbonates, charcoal, or sand. The lower boundary is slightly wavy and sub-horizontal at a depth of 325cm.

BD4-2: 325 – 412 cm

Unit BD4-2 is porous silty loam with layers and lenses of medium to coarse sand. The unit has very weak sub-angular blocky structure in the upper portion. The unit contains shells, Fe/Mn nodules (up to 2mm in diameter) and Fe mottling (up to 8mm in diameter). The unit is also stratified with sandy layers (~1cm thick) every 5cm to 15cm. From the top to the bottom the layers become wavier and crossbedded and the abundance of nodules and mottling increases. The unit has a sharp lower boundary at a depth of 412cm.

BD4-1: 412 – 440 cm (bottom of trench 4)

Unit BD4-1 is fluvial sand and gravel. The grains are coarse sand and pebbles that are generally up to 5cm along the long axis. The largest in situ grain was ~10cm along the long axis. The unit had variable colour and mineralogy and extended below the bottom of the trench at 440cm.

Using the main buried soil as a datum, the lesser developed soils as marker units, and the unit descriptions, the three trenches where then correlated to create a complete depositional history and pseudo-section (figure 4.2). It should be noted that the main buried soil underwent varying degrees of pedogenesis depending on whether it was at the top of a plateau or the base of a paleo-depression. This is likely due to the bottom of a

paleo-depression having a higher moisture content and therefore undergoing stronger soil formation. This complete section was then used for the correlation of the magnetic studies and the grain size analysis as well as the development of the age model. The age model could then be used to determine the frequency of the climate cyclicity and allows for the comparison to other Holocene climate studies.

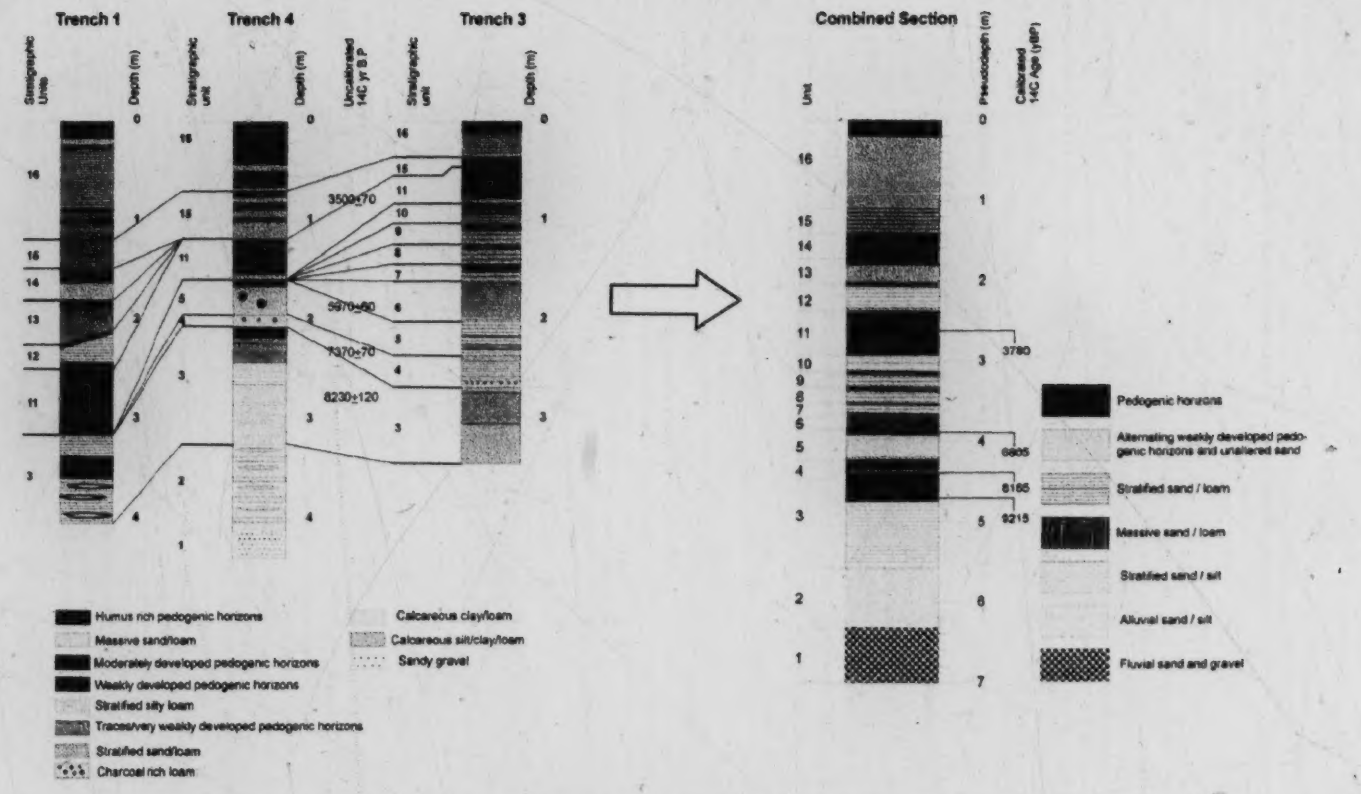

Figure 4.2 Correlation of trenches 1, 3, and 4 results in a complete pseudo-section comprising all 16 units described at the Burdukovo site.

Chapter 5.1 Age Model

The age model was created in order to convert from depth to age. This would allow to us to apply an age to our magnetic and grain size data. Since the magnetic data and grain size data represent changes in climate, applying an age model to them will allow us to determine whether they contain any known periodicities. Once the age model is calculated and applied to the Burdukovo site, the results could be compared to data from other sites. The most specific application of the age model is to calculate and compare the changing parameters (FD and grain size) with respect to depth and age from the Burdukovo site with North Atlantic data (oxygen isotope and insolation) with respect to age.

The age model was created using samples that were taken from a trench that was dug as part of the first expedition to the study site in the summer of 2001. The original trench from 2001 was located directly beside trench 4 of the 2004 study. The samples that were dated were charcoal fragments. The samples were tested using the Accelerated Mass Spectrometry (AMS) technique for ^{14}C dating and the testing was carried out by Beta Analytical, Inc. The oldest sample was taken from unit 3 and yielded an uncalibrated age of 8230±120 yBP. The second oldest sample was taken from the boundary between unit 3 and unit 4 and gave an uncalibrated age of 7370±70 yBP. The third oldest sample was from the top of unit 5 and gave an uncalibrated age of 5970±60 yBP. The youngest sample was taken from the middle of unit 11, the main buried soil, and yielded an uncorrected age of 3500±70 yBP. The uncalibrated dates obtained then required calibration due to the practice of labs using the Libby half-life when determining age and also due to variability of atmospheric ^{14}C levels due to climate changes as well as

variability in solar radiation causing changes in the atmosphere. The original ^{14}C half-life of 5568±30 years determined by Arnold and Libby (1949) is still used by laboratories when comparing raw data. The variability of atmospheric ^{14}C is due to a combination of solar fluctuations and vocalic activity dumping radiocarbon depleted CO_2 into the atmosphere. Corrected ^{14}C dates are determined by measuring ^{14}C levels in organic material of a known age such as tree rings. The thickness of tree rings is representative of the amount of ^{14}C in the atmospheres during that year of a trees life (Bronk Ramsey, van der Plicht and Weninger, 2001). The atmospheric levels of ^{14}C are determined and a calibrated scale is calculated. A new ^{14}C date is calibrated by matching the uncalibrated date with the curve to determine the best possible calibrated ^{14}C date.

The uncorrected ^{14}C dates were calibrated using the OxCal version 3.10 (© copyright Bronk Ramsey, 2005) software developed by the University of Oxford. This software was used because it is made available to the public free of charge and provides a quick and easy way to calibrate ^{14}C dates. The oldest sample gave a calibrated age of 9215±185 yBP (Bronk Ramsey, 1995; Bronk Ramsey, 2001; Reimer et al., 2001) and the second oldest sample gave a calibrated age of 8185±165 yBP (Bronk Ramsey, 1995; Bronk Ramsey, 2001; Reimer et al., 2001). The third oldest sample gave a calibrated age of 6805±145 yBP (Bronk Ramsey, 1995; Bronk Ramsey, 2001; Reimer et al., 2001), and the youngest sample was calibrated at 3780±90 yBP (Bronk Ramsey, 1995; Bronk Ramsey, 2001; Reimer et al., 2001).

Using the thickness between samples and the changes in age, sedimentation rates were determined from 9215 yBP to the present. The sedimentation rate from 9215 yBP to 8185 yBP was determined to be 31.6 cm/ky. From 8185 yBP to 6805 yBP the

sedimentation rate was calculated to be 36.2 cm/ky. From 6805 yBP to 3780 yBP the sedimentation rate was determined to be 41.3 cm/ky. For the sedimentation rate from 3780 yBP to the present the thickness between the main buried soil and the top of the modern soil in trench 1 was used and the age of the top of the modern soil was taken to be the present. The reason the thickness in trench 1 was used was that it allowed us to determine the maximum sedimentation rate. Using the larger depositional rate resulted in more data points in the same time frame as a smaller depositional rate. Another reason is that there are units above the main buried soil that are represented in trench 1 that are not observed in trench 3. By using the thickness of units in trench 1 to determine for the rate of deposition, we can more easily observe the warming and cooling periods that have occurred since the warm period responsible for the main buried soil. The maximum sedimentation rate from 3780 yBP to the present was calculated to be 69.5 cm/ky.

For the age model, the rate of deposition was taken to be linear between sequential calibrated dates. The sedimentation rates are average because they assign the same rate to both soil and loess units that are within the same age range, even though loess units have a higher rate than soil units. A linear rate of deposition is used because there are only four ^{14}C dates available for determining the age model. As well, if we did not use a linear rate of deposition between ^{14}C dates, then a rate of deposition for either loess or soil units would have to be arbitrarily chosen in order to determine the rate of deposition for the other. Doing this could result in even greater error in the age model. The method we chose to use is the standard method for creating an age model and will result in slight errors, however these errors are not significant enough to affect the spectral analysis. For the entire section, the maximum rates of deposition were calculated. This resulted in an

elevated rate of sedimentation for the last 3.78 ky, as the thickest section from the main buried soil to the present day surface occurred at the thickest part of a paleo-depression. Because the deposition was occurring in a paleo-depression, the rate of deposition is exaggerated to a value of 69.5 cm/ky. If the rate had been calculated at the plateau that occurs in trench 3, the resulting rate of deposition would have been much lower, approximately 16.5 cm/ky. This makes the average depositional rate for the last 3.78 ky approximately 43 cm/ky, which is similar to the rates for the previous 5.5 ky.

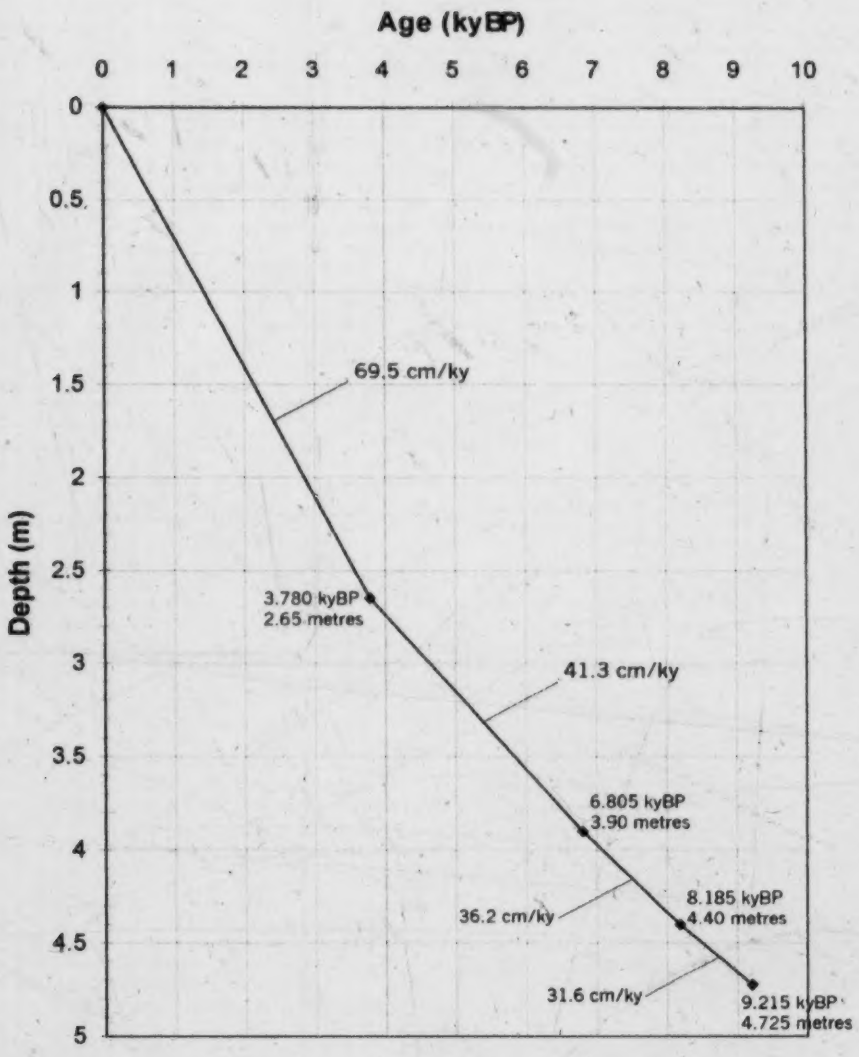

Figure 5.1.1 Age model showing an increase in sedimentation rates through the Holocene.

Chapter 5.2 Magnetic Susceptibility and Grain Size Analysis

For typical loess/soil sequences, the magnetic susceptibility shows highs for the soil horizons and lows for the loess units. This is because for typical loess/soil sequences the input of magnetic material from the source area is relatively constant and the change in magnetic susceptibility is due primarily to bacterial activity during pedogenesis. In Chinese loesses, this correlation between magnetic susceptibility and unit type is very distinct (Liu et al., 1992; Sartori et al., 1999). This can also be seen in other Eurasian deposits such as those in the Ukraine (Tsatskin et al., 1998) and in Tajikistan (Forster and Heller, 1994). It may be that the loess/soil sequence at the Burdukovo site could also show soil units with a high magnetic susceptibility and loess units with low magnetic susceptibility. However, looking at the results from trench 1 we see that there is no correlation between unit type and magnetic susceptibility. For example, from 0.5m to 1.15m the magnetic susceptibility shows distinct peaks in magnetic susceptibility in a stratified sand unit that shows no evidence of pedogenesis. As well, from 1.5m to 2.1m there are no peaks in magnetic susceptibility while there are two soil horizons that occur within that interval. What this indicates, is that the magnetic susceptibility is being strongly affected by the wind strength as well as pedogenesis. Stronger winds are entraining larger magnetic particles and transporting them from the source area to the depositional area. This results in the loess units potentially having a higher magnetic susceptibility than the soil units. The inverse correlation between high magnetic susceptibility with soil units and low magnetic susceptibility with loess units is also seen in Siberian loess/paleosol sequences from the Kurtak site in the Yenisey River valley (Chlachula et al., 1998) as well as Alaskan loess/soil deposits in Alaska (Begét et al.,

1990). This is because the magnetic susceptibility is highly dependent on the wind and sediments that that the wind deposits at the sites. At the sites in Alaska and at Kurtak, the stronger winds during glacial periods are strong enough to transport heavier magnetic particles with the other sediments. Enough magnetic material that the amount deposited is comparable to the amount of superparamagnetic material produced during soil formation. This results in a lack of correlation between magnetic susceptibility and loess/soil units. Because of this, the parameter of frequency dependence (FD), as discussed in chapter 3, is used to distinguish between loess and soil horizons. This parameter has been used before to successively show the correlation between magnetic properties and soil formation for Pleistocene loess sequences of Western and Central Siberia (Kravchinsky et al., 2007). Testing samples for both high and low frequency susceptibility did reveal a change in frequency dependent susceptibility between the two types. Loess units showed a low FD and soil units showed a high FD (figures 5.2.1-5.2.3). Values for loess units were less than 1%, while peak values for buried soils typically varied from approximately 1.3% to 5.3% in more developed units (Table 1). These are relatively low values for FD, but that is typical of Siberian loess deposits (Chlachula et al., 1998; Kravchinsky et al., 2007). Because of the low FD, the noise in the magnetic analysis looks significant. To compensate for this the mean FD was calculated along with the mean plus one standard deviation. FD values below the mean were considered to be base level FD while values greater than the mean plus one standard deviation correlated with soil horizons. Grain size analysis showed loess units having a coarser grain size with highly variable median diameters that ranged from around 15μm to 55μm and modal diameters that ranged from 35μm to 65μm. Buried soils had median

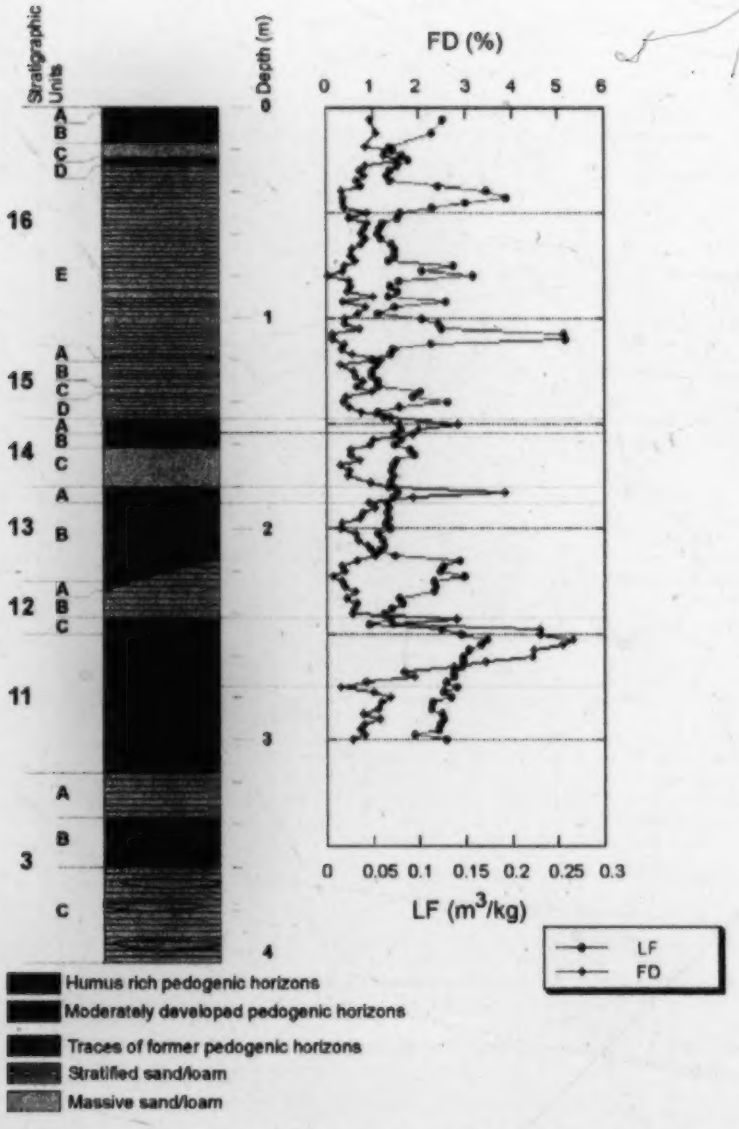

Figure 5.2.1 Stratigraphy and magnetic measurements for trench 1 at the Burdukovo site. Low frequency magnetic susceptibility (LF) does not show any consistent correlation to soil units while the frequency dependence (FD) shows spikes that can be correlated with the stratigraphy.

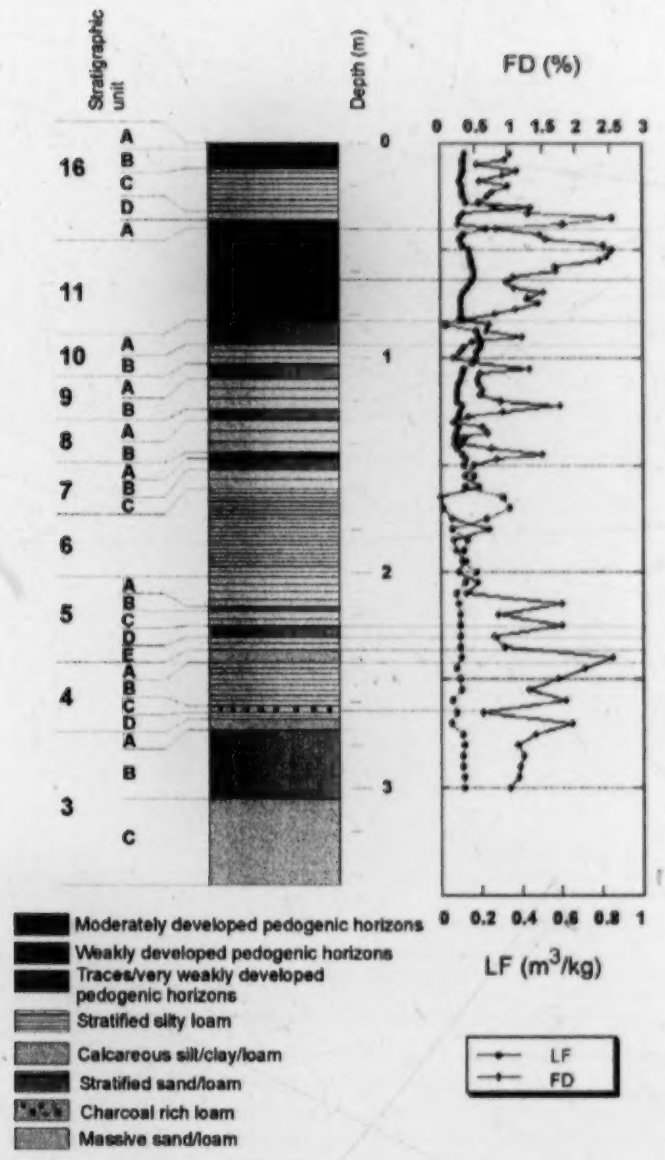

Figure 5.2.2 Stratigraphy and magnetic measurements for trench 3 of the Burdukovo site. Soil horizons show a high FD. The main buried soil (unit 11) shows a very prominent spike in FD.

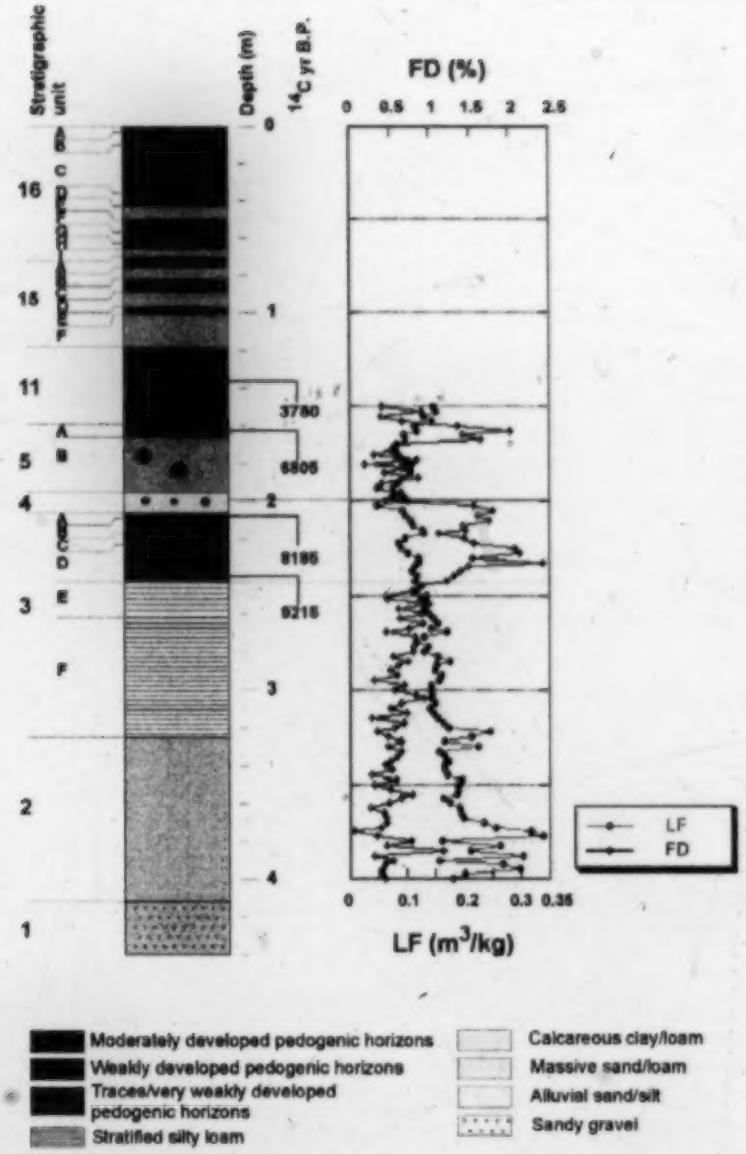

Figure 5.2.3 Stratigraphy and Magnetic measurements for trench 4 at the Burdukoyo site. The calibrated ^{14}C age dates that were used to develop the age model are also included.

diameters that were generally less than 12μm and modal diameters that were less than 15μm. Loess units were also more poorly sorted, showing a difference in modal and median diameters of up to 30μm for individual samples and a larger maximum grain size, often greater than 1mm. Buried soils were more well-sorted and modal and median diameters were within approximately 4μm of each other for individual samples. The maximum grain size for buried soils was generally 250μm or less. Grain size analysis data can be found in table 2, table 3, and table 4.

The FD and the correlated units from all three trenches were also stacked into a complete section (figure 5.2.4). What figure 5.2.4 shows is for the soil at the top of unit 14, there is a corresponding high in FD as well as a low in median grain size. At the top of unit 13 there is another soil horizon that also shows a peak in FD and a low in median grain size. At the top of unit 12 there is a very thin, and weakly developed soil horizon that has a small peak in FD but no low in the median grain size. This is due to the thickness of the unit being smaller than the sample size, which resulted in material from loess units above and below being included in the sample. Unit 11, which was the most strongly developed buried soil, also showed the highest FD as well as very low median grain size. Soil horizons at the tops of units 9 and 8 also show moderate peaks in the FD and moderately low median grain sizes. At the top of units 7 and 5 the soil horizons show moderate peaks in FD and lows in median grain size. From the top of soil horizon in unit 4, through to the bottom of the soil in unit 3 consistent highs in FD and lows in median grain size are seen with the exception of a couple data points that correspond to a very thin sand layer at the bottom of unit 4.

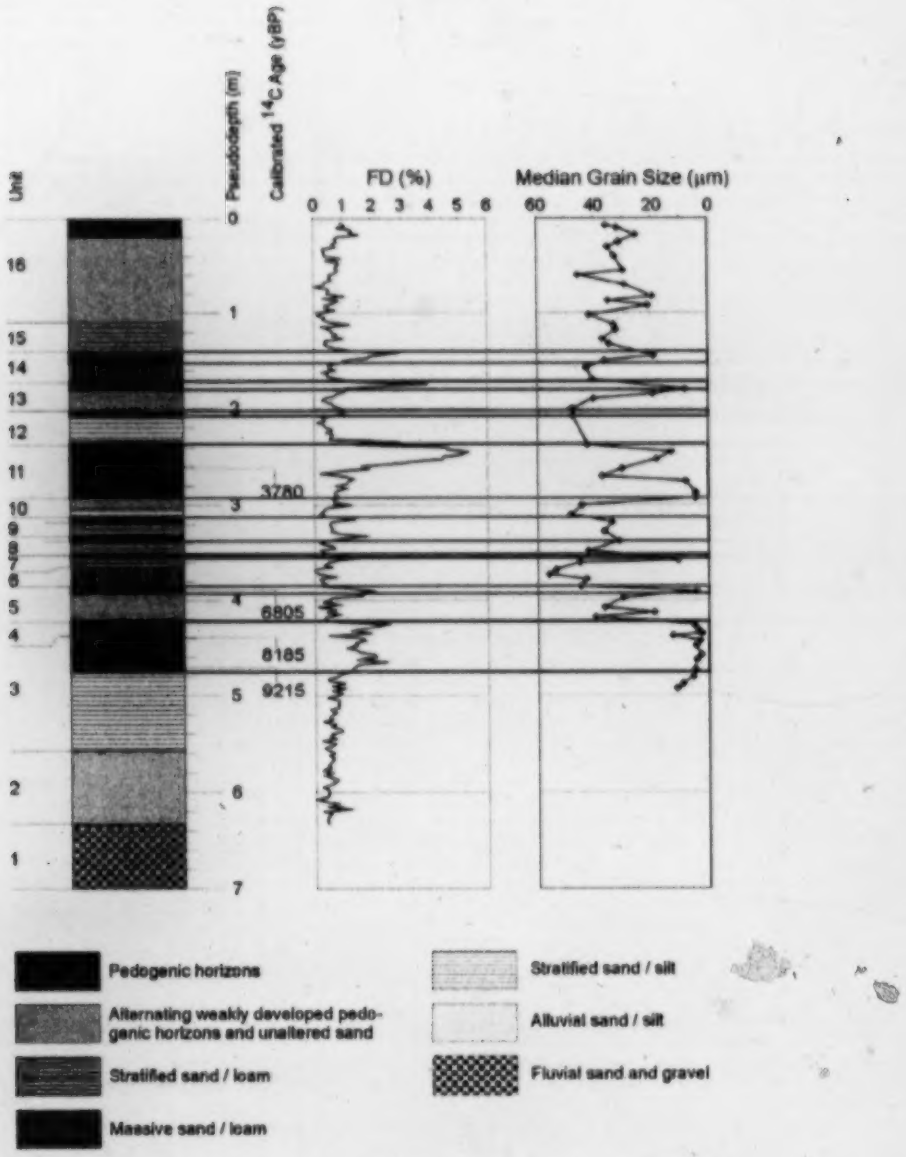

Figure 5.2.4 Complete stacked and simplified stratigraphic section for the Burdukovo site with FD. Pedogenic horizons are correlated with highs in FD. The calibrated ^{14}C dates are included with the completed section.

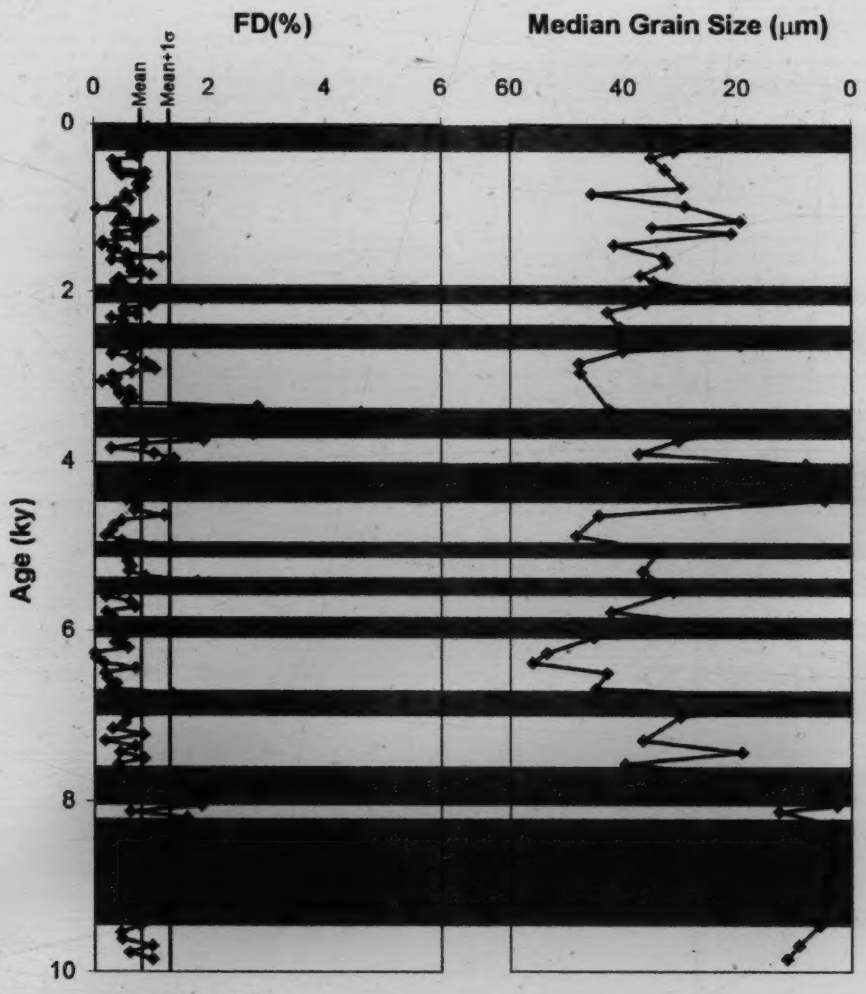

Figure 5.2.5 FD and median grain size plotted with respect to age. Gray shaded areas indicate areas highs in FD that also correlate with highs in median grain size.

The complete and stacked section also included calibrated ages, so that the age model that was developed, as discussed in chapter 5.1, could be applied in order to determine

approximate ages of the different units. The FD and grain size analyses were then plotted with respect to age (figure 5.2.5). The FD shows distinct increases at approximately 2.0, 2.5, 3.7, 5.0, 5.6, 6.0, and 6.8 kyBP and an overall increase after 7.8 kyBP (figure 5.2.5). The grain size analyses show lows in median grain size after 2.0 kyBP at approximately 2.1, 2.7, 3.8, 4.4, 5.0, 5.7, 6.0, 6.8, and 7.4 kyBP and an overall decrease after 7.8 kyBP (figure 5.2.5). The magnetic susceptibility and grain size analysis results from the Burdukovo site were consistent with each other (figure 5.2.5), meaning that peaks in FD corresponded to lows in median grain size.

Chapter 5.3 Magnetic Mineralogy

In addition to the FD and the grain size analysis a high temperature magnetic susceptibility was attempted on several samples as well as the isothermal remanent magnetization (IRM). The purpose of this was to determine the magnetic mineralogy of the deposits. If the magnetic mineralogy of the loess units is predominantly magnetite, then this would also explain the high magnetic susceptibility of the loess units.

The samples being tested for the high temperature magnetic susceptibility were measured using a Bartington MS2W system. The temperature of the samples was increased from room temperature to 700°C and the magnetic susceptibility was measured every 2°C. Once the samples had finished heating to 700°C, they were allowed to cool to room temperature and the magnetic susceptibility was taken at 2°C increments. The samples all show an increasing magnetic susceptibility to a temperature of approximately 380°C. At 380°C all samples show a change in the rate of increasing magnetic susceptibility. Samples BD1-92.5 and BD1-107.5 actually show slight decreases in magnetic susceptibility until the temperature reaches approximately 340°C to 350°C, at which point the magnetic susceptibility begins to increase again. The samples increase in magnetic susceptibility until the temperature reaches approximately 555°C and all show sharp decreases from 570°C to 580°C. This is due to the Curie temperature of magnetite and the relatively high concentration of magnetite present in the sample with respect to other magnetic materials. Sample BD1-92.5 (figure 5.3.1) peaked at a temperature of 554°C and a magnetic susceptibility of 0.219 m^3/kg. Sample BD1-107.5 (figure 5.3.2) peaked at a magnetic susceptibility of 0.390 m^3/kg at temperatures from 356°C to 358°C.

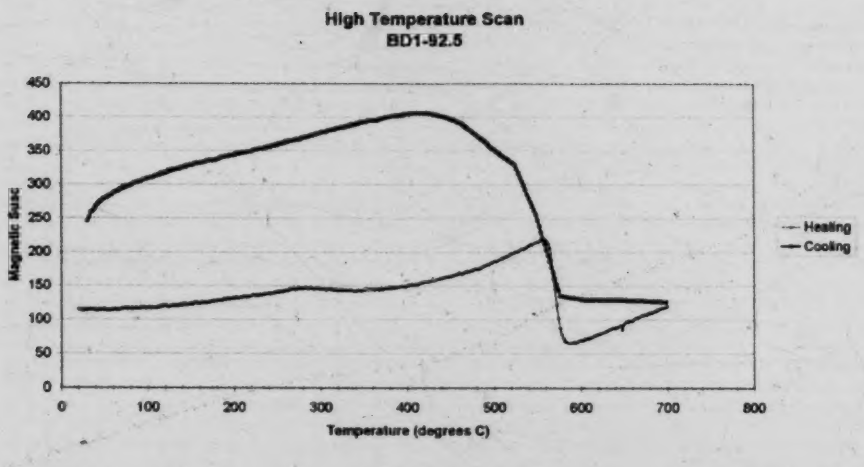

Figure 5.3.1 Magnetic susceptibility measurements of sample BD1-92.5 as temperature was increased from room temperature to 700°C (red line) and cooled from 700°C back to room temperature (blue line).

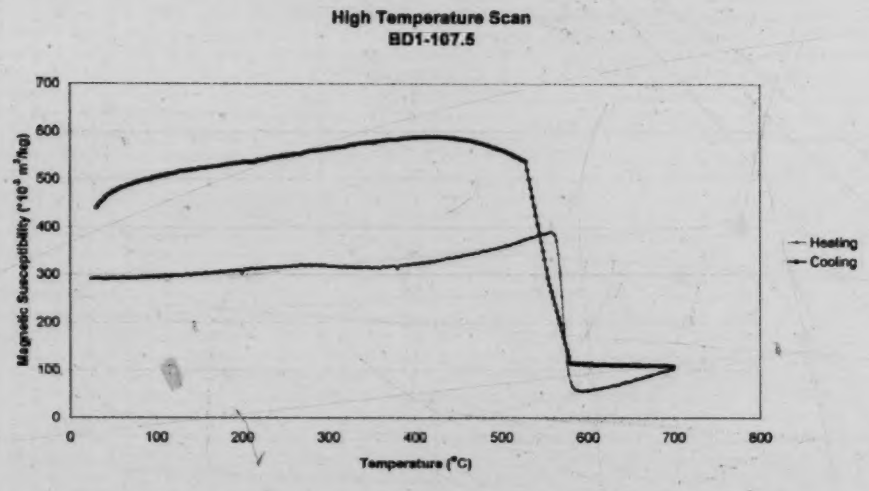

Figure 5.3.2 Magnetic susceptibility measurements of sample BD1-107.5 as temperature was increased from room temperature to 700°C (red line) and cooled from 700°C back to room temperature (blue line).

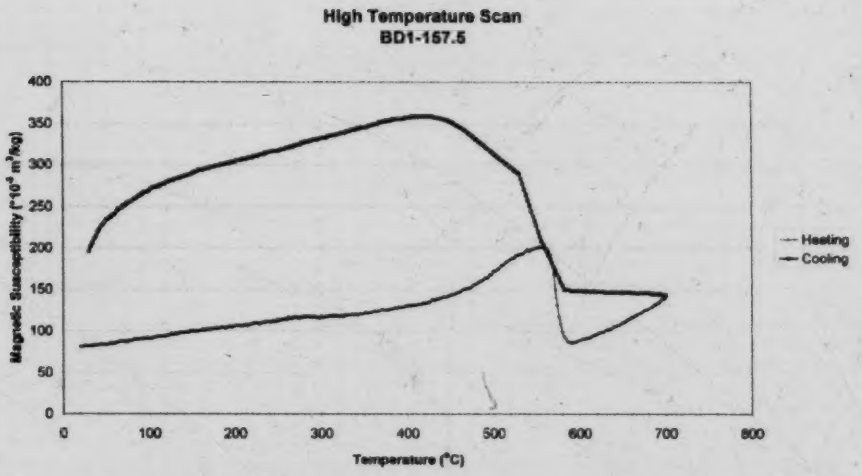

Figure 5.3.3 Magnetic susceptibility measurements of sample BD1-157.5 as temperature was increased from room temperature to 700°C (red line) and cooled from 700°C back to room temperature (blue line).

Sample BD1-157.5 (figure 5.3.3) peaked at a temperature of 358°C and a magnetic susceptibility of 0.202 m^3/kg. All samples showed a change in the increase in magnetic susceptibility at approximately 270°C, samples BD1-92.5 and BD1-107.5 actually show a decrease in magnetic susceptibility. Others have previously interpreted this anomaly as a thermally triggered change of metastable maghemite (γ-Fe_2O_3) to hematite (α-Fe_2O_3) (Zhu et al, 2003). The anomaly observed in our samples is much smaller than is observed in other studies and indicates that any maghemite present is likely present in only trace amounts. After reaching minimum magnetic susceptibilities at approximately 590°C, all samples started to steadily increase magnetic susceptibility to our end temperature of 700°C. The increase in magnetic susceptibility after 590°C is likely due to the presence of hematite, either initial hematite or hematite produced by the reduction of maghemite at

increased temperature. The samples tested were all from loess units, and therefore if hematite is present, it was not converted to magnetite through bacterial activity during soil formation. If it were, then we would see a correlation between magnetic susceptibility and change between loess and soil units. Whether the increase is due to hematite or the oxidation of magnetite can be confirmed by measuring the magnetic moment of various samples and exposing them to an increasing magnetic field. This procedure was performed and described in greater detail later in this chapter. The samples were then allowed to cool, and the magnetic susceptibility remained relatively constant until the temperature drops to approximately 580°C. From 580°C to approximately 525°C, the magnetic susceptibility increases rapidly in all samples. From 525°C to 430°C, the magnetic susceptibility continues to increase but at a much slower rate. After the temperature has dropped to approximately 430°C, the magnetic susceptibility levels off for approximately 10°C and then begins to continually decrease until the sample reached ambient temperature.

The magnetic moment for several different samples was also tested. Once the initial magnetic moment was measured, each sample was then placed in a positive magnetic field (with respect to a positive z-axis) that was increased. After the samples were placed in the magnetic field, the sample was removed and the magnetic moment was measured. Once the sample was saturated, the sample was then placed in a reverse field and then measured. The data was then tabulated (table 5) and plotted (figure 5.3.4). Sample BD1-25 was measured in a spinner magnetometer and the inducing field was created using a manually controlled IRM. The other samples were measured using the Superconducting Rock Magnetometer purchased from and installed by 2G Enterprises. The inducing field

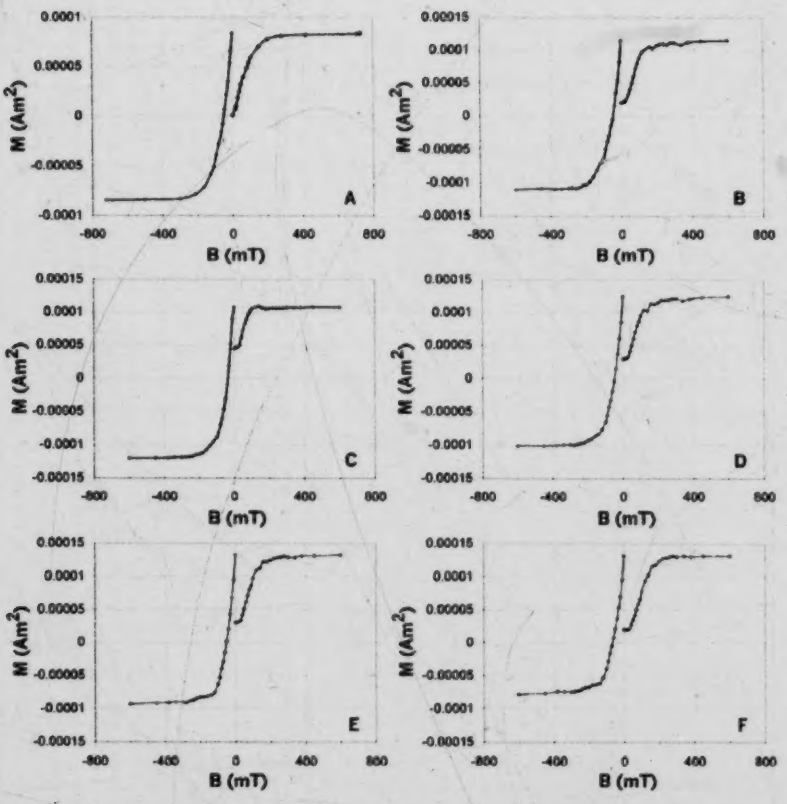

Figure 5.3.4 Magnetic moment of Burdukovo samples when placed in an inducing magnetic field.

(A) Sample BD1-25 shows saturation of the magnetic moment when the inducing field reaches ~300mT. (B) Sample BD1-230 shows saturation of the magnetic moment when the inducing field reaches ~200mT. (C) Sample BD1-260 shows saturation of the magnetic moment when the inducing field reaches ~120mT in the positive direction and ~200mT when the field is in the negative direction. (D) Sample BD3-40 shows saturation of the magnetic moment when the inducing field reaches ~200mT in the positive direction and ~300mT when the field is in the negative direction. (E) Sample BD3-55 shows saturation of the magnetic moment when the inducing field reaches ~200mT in the positive direction and ~300mT when the field is in the negative direction. (F) Sample BD4-200 shows saturation of the magnetic moment when the inducing field reaches ~250mT.

that the samples were placed in was produced by a model 2G660 Pulse Magnetizer that was also purchased from and installed by 2G Enterprises. This allowed for greater control over the inducing field that the final five samples were exposed to.

Sample BD1-25 was from unit BD1-16 and is from the modern soil. The sample showed a steady increase in magnetic moment and reached saturation when exposed to an inducing field of approximately 300mT. The field was then reversed and the sample again reached saturation at approximately -300mT (figure 5.3.4A). Sample BD1-230 was from unit BD1-12 and is a loess sample. The sample reached saturation at just over 200mT in both directions. Sample BD1-260 was from unit BD1-11 and is from the main buried soil. The sample reached saturation at approximately 120mT in the positive field and at approximately -200mT in the reverse field (figure5.3.4C). Sample BD3-40 was from unit BD3-15 and is a very weakly developed soil. The sample reached saturation at approximately 200mT in the positive field and at approximately -300mT in the reverse field (figure5.3.4D). Sample BD3-55 was from unit BD3-11 and is from the main buried soil. The sample also reached saturation at approximately 200mT in the positive field and at approximately -300mT in the reverse field (figure5.3.4E). Sample BD4-200 was from unit BD4-4 and is from a loess unit. The sample reached saturation at approximately 250mT in both directions (figure5.3.4F).

Because the magnetic moment of both loess and soil samples were able to be saturated before the magnetic field reached 400 mT in either direction indicates that the principal magnetic material present is magnetite. If initial hematite were present in measurable quantity, saturation of the magnetic moment would not be achieved. This confirms that observation in the high temperature magnetic susceptibility of increasing magnetic

susceptibility from 590°C to 700°C is due to the presence of hematite due to reduction of maghemite to hematite and not due to original hematite at the depositional site.

Chapter 5.4 Correlation of Regional and Global Holocene Data

The loess soil sequences at the Burdukovo site follow a wind vigour model of deposition. This means that the magnetic susceptibility of the units is not as effective indicator of climate change. Instead, the frequency dependent (FD) must be used as the proxy for climate variability. This is because in a wind vigour depositional setting, the magnetic susceptibility is highly variable depending on the wind strength. Changes in FD, on the other hand, are independent of wind strength, variability instead being due to pedogenic processes. The comparison of the FD with the median grain size supports a wind vigour driven depositional environment. Therefore, during soil forming processes we have weaker winds entraining material from the source area and carrying them to the depositional site resulting in a smaller median grain size during times of pedogenesis. As for FD, during warmer periods of soil formation bacterial activity utilizes the Fe from larger and less magnetically susceptible grains and produces superparamagnetic magnetite grains resulting in an increase in FD during times of pedogenesis. Therefore we expect that an increase in FD will correspond to a decrease in median grain size. Figure 5.4.1 demonstrates that this is indeed the case. For ease of correlation, the grain size axis on the median grain size chart has been inverted so that we could compare spikes in FD with spikes in median grain size. Between 2kyBP and 10kyBP there is remarkable correlation between the FD and median grain size. Peaks in the FD at approximately 2.0, 2.5, 3.6, 5.0, 5.4, 6.0, 6.9, and from 7.8 to 9.3 ky correlate directly to lows in the median grain size. There is one peak in median grain size at approximately 4.4 kyBP that does not correlate with a well-defined spike in the FD. There is also a spike in median grain size at approximately 7.4 kyBP that does not correspond to any

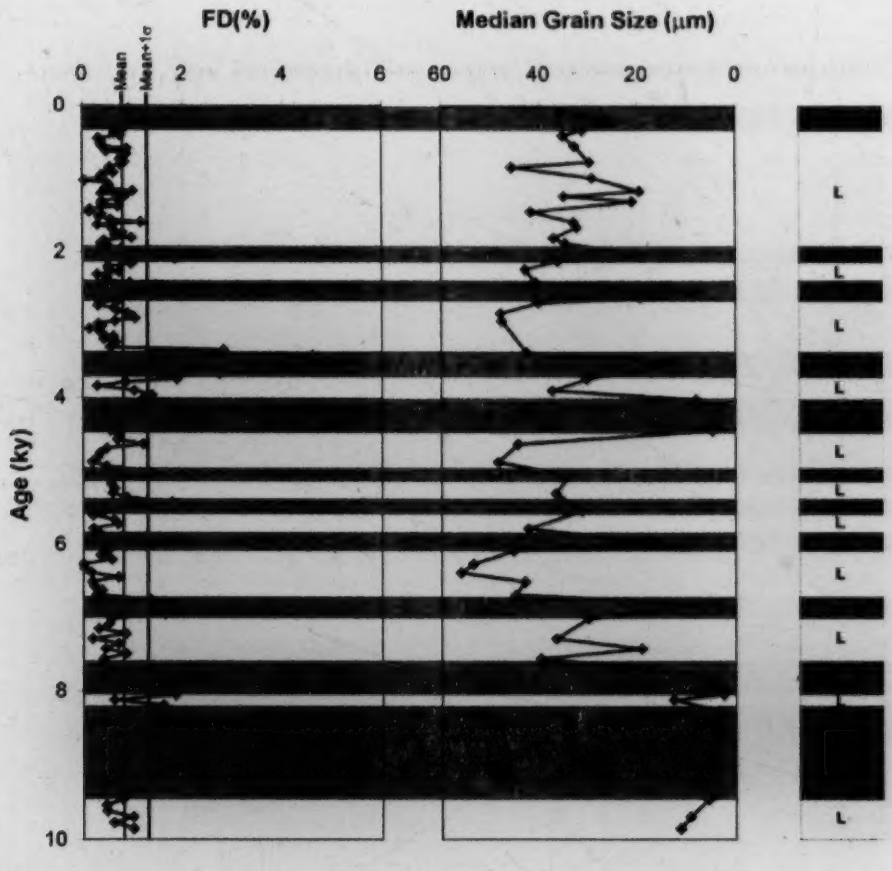

Figure 5.4.1 Comparison of the frequency dependent percent and the median grain size from the Burdukovo site. Highs in FD generally correspond to decreases in median grain size. The mean was determined using all FD samples that had a value less than 2.5 and represents the background noise, or base level, FD. The red line indicates the mean plus 1 standard deviation (σ). Any peaks above the mean + 1σ are considered prominent and correspond to a buried soil (S) in the simplified stratigraphic sequence on the right. The loess unit are marked as L.

significant increase in FD. However, the spike in median grain size is cause by a single sample and may be due to contamination from other units through post depositional disturbance such as burrowing.

Once the mechanism of deposition was determined, the results from Burdukovo were compared to results from the North Atlantic and from Lake Baikal. The study from Lake Baikal that are used in the attempt to correlate our data with regional records is diatom concentrations (Morley et al. 2005) and magnetic susceptibility of sediments (Boes et al. 2005). The records from the North Atlantic that have been used for comparison with the global record are the normalised and smoothed $\delta^{18}O$ record of GISP2 data and a summer insolation curve with a 900 year component from Schulz and Paul (2002). In the $\delta^{18}O$ data set, an increase indicates warmer periods. This is because during warmer periods the amount of water vapour in the atmosphere also increases and therefore the total amount of ^{18}O. When the water precipitates out, the molecules with ^{18}O precipitate out first thereby increasing the ratio of ^{18}O to ^{16}O. This ratio of ^{18}O to ^{16}O is the value represented by $\delta^{18}O$. In colder areas, such as those with glaciers, this precipitation can be in the form of snow and can be incorporated into the glacier. This is how ^{18}O records from glaciers can be used as climatic indicators. The insolation curve is a 900 year cycle of varying solar radiation that can have an effect on climate where highs indicate warmer periods and lows represent colder periods.

The comparison between the FD and median grain size from Burdukovo with the $\delta^{18}O$ of the GISP2 shows good correlation (figure 5.4.2). At 2.0, 3.8, 6.0, 6.9, 7.7, and 8.4 kyBP highs in the $\delta^{18}O$ correspond to both an increase in FD and median grain size. There is a high in $\delta^{18}O$ at approximately 5.2 kyBP that does not correspond to a distinct increase in

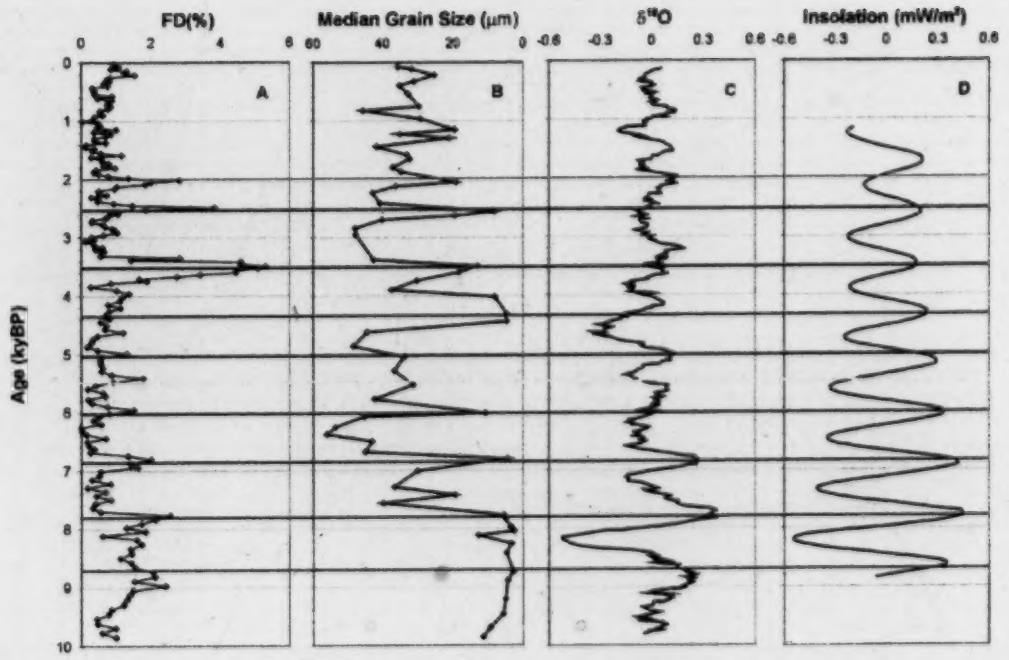

Figure 5.4.2 Correlation of (A) Burdukovo FD data, (B) median grain size, (C) smoothed and normalized GISP2 oxygen isotope data (Schulz and Paul, 2002), and (D) solar insolation with a 900 year component (adapted from Schulz and Paul, 2002). The red lines indicate warmer trends seen in the Burdukovo data that also correspond to warmer trends in the $\delta^{18}O$ and in the insolation curve. The yellow lines indicates peaks in both the FD and median grain size that can be correlated with a rise in the $\delta^{18}O$ data, but does not correlate with the insolation curve.

FD but does correlate to an overall decrease in median grain size at the same time. As well, the decrease in median grain size at approximately 4.4 kyBP correlates closely to a high in $\delta^{18}O$. There is an increase in FD and a decrease in median grain size at approximately 2.5 kyBP that does not correspond to an increase in $\delta^{18}O$ in the GISP2 data. This spike in the Burdukovo data does correspond to a high in the summer insolation curve. The highs in FD and lows in median grain size at 2.5, 3.8, 6.0, 6.9, 7.7, and 8.4 kyBP all correspond to highs in the summer insolation curve. The spike at 2.0 that correlates to a high in $\delta^{18}O$ does not occur at a high in the summer insolation curve but in between the previous high and the subsequent low. The high in the summer insolation curve that occurs at approximately 4.4 kyBP does not correlate with any well defined increase in FD but does correspond to a significant decrease in median grain size. There is also a high in the summer insolation curve at approximately 5.2 kyBP that does not correlate with an increase in FD but does correspond to an overall decrease in median grain size.

What can be seen from the various data sets is that there is excellent correlation for almost all the peaks. It is possible to conclude that the warming and cooling trends of the Holocene at our Siberian site were global in nature rather than regional. The few peaks that show lack of correlation between the North Atlantic data and the Burdukovo data is likely due to variations between marine and mid-continental depositional and climate settings.

5.5 Spectral Analysis

A spectral analysis was performed on the results of the magnetic study and the grain size analysis of the Burdukovo study. A spectral analysis was also performed on the North Atlantic oxygen isotope data, insolation curve, and Lake Baikal results. The purpose of this procedure was to determine if any periodicity displayed by the Burdukovo data match that shown by other studies.

The spectral analysis was performed on the frequency dependence and the median grain size using AnalySeries software version 1.2.2 (Paillard et al., 1996). A cross-correlation was also performed on the FD and the median grain size to determine the coherence between the two parameters. A spectral analysis was also performed on the studies that were used for comparison. The studies that were used for comparison were Morley et al. (2005) and Schulz and Paul (2002). The study by Morley et al. (2005) was chosen for comparison because it looks at the concentration of diatoms in Lake Baikal over the last 15.7ky. As the climate changes, so does the concentration of diatoms in the lake. This provides a local record of Holocene climate that can be compared to the Burdukovo study. The Schulz and Paul study created a used oxygen isotope data from Grootes and Stuiver (1997) and compared them to summer insolation curve with a 900 year cycle based on Loutre et al. (1992). These data sets were chosen because they are marine Holocene climate records that can be compared to the continental record and can show that the climate change is global in nature. We performed separate frequency analyses on the isotope data and the insolation curve and then compared the results to both the Morley study and our own.

The analysis performed on all data was a Blackman Tukey spectral analysis and

parameters such as resampling interval, confidence interval, frequency range, and step interval were kept consistent. The Blackman-Tukey method was used as it is the standard auto-correlation method when estimating the power spectrum of a time series. The Blackman-Tukey method opts for robustness at the expense of resolution. For the AnalySeries software that was used to perform the spectral analysis, it is one of the preset methods for computing the autocovariance of the data. It then applies a window to smooth the results and performs a Fourier transform calculate the power density of the spectra (Paillard et al, 1996). The window that was applied to the data was a Tukey window. The power density, or power as it appears in figures 5.5.1 and 5.5.2, is the result of the input data and are independent of the other analysis. This means that the power from one analysis cannot be compared to the power of another analysis as the input values are unrelated. The power basically refers to the strength of agreement of the data at a particular frequency.

For each data set the data was first prepared for the analysis by resampling at an interval of 0.02ky. A resampling interval of 0.05ky was also used and resulted in identical results for the Burdukovo data. The reason 0.05 and 0.02ky intervals were chosen was because the FD data set, the larger of the data Burdukovo data sets, contained approximately 200 data point spanning 10ky. This translated to 0.05 ky/data point. However, the GISP2 data set contained 500 data points for the last 10ky, or 0.02 ky/data point. For this reason the resampling interval of 0.02ky was used. The data sets were resampled using linear interpolation. The data set for the FD and the median grain size included data from the present to 9.85 kyBP. This is the oldest known date for the Burdukovo data and is situated in the oldest buried soil. The rate of sedimentation prior to that is unknown and

since it included the oldest buried soil, interpolated to an older date was attempted but not included. This is because inclusion of the older dates would be pure speculation.

The spectral analysis performed on the median grain size revealed peaks at approximately 0.23, 0.67, 1.17, and 2.06 cycles/ky (figure 5.5.1A). This translates to periods of 4.36, 1.49, 0.85, and 0.48 ky respectively. The spectral analysis on the FD revealed prominent peaks at frequencies of approximately 0.23, 0.67, 1.08, and 2.06 cycles/ky (figure 5.5.1B). This translates to periods of 4.36, 1.49, 0.93, and 0.48 ky respectively. The grain size and the FD spectral analysis were also normalised and compared to all other Holocene frequency analyses. The data sets were normalised by calculating a trendline, then subtracting the trendline from the data set. The reason for detrending the data sets is that the peaks in the frequency are more pronounced once the trend has been removed. This allows for easier correlation between the different frequency analyses. For the spectral cross-correlation that was performed, the confidence interval was set at 95% and the data sets were resampled from 0 to 3 cycles/ky with a step interval of 0.02. The coherence between the two analyses was very consistent and varied from a maximum value of 0.90 to a minimum of 0.69 (figure 5.5.1C). This shows that there is good correlation between FD and median grain size. The spectral analysis performed on Baikal diatom concentration from Morley et al. (2005) included data to 9.84 kyBP. The spectral analysis of the Baikal diatom concentration also shows a prominent peak at 0.23 cycles/ky and slight peaks at approximately 0.9, 1.3, and 2.06 cycles/ky (figure 5.5.2C). The spectral analysis of the diatom concentration study results in periods of 4.36 and 0.48 ky that agree with our longest and shortest periods, the other peaks reveal periods of 1.1 and 0.77 ky that are shorter than our observed periods. The diatom spectral analysis was

also normalised using the same procedure as was used on the Burdukovo data. The oxygen isotope data set from Schulz and Paul (2002) contained data well beyond the 9.85 kyBP that was used for the spectral analysis of the FD and median grain size, but to be consistent, only Holocene data to 9.8 kyBP was used. The analysis showed a prominent peak at approximately 1.05 cycles/ky, a significant peak at 0.6 cycles/ky, and a slight peak at approximately 1.9 cycles/ky. This results in periods of approximately 0.95, 1.67, and 0.53 ky respectively (figure 5.5.2D). The data set for the insolation curve from Schulz and Paul (2002) only contained data to 8.9 kyBP. The results of the spectral analysis performed on the insolation curve revealed a prominent peak at approximately 1.15 cycles/ky and slight peaks at approximately 0.5 and 1.8 cycles/ky. The resulting periods are 0.87, 2, and 0.55 ky respectively (figure 5.5.2E). This result was expected, as an insolation curve with a 900-year component would be expected to yield a symmetrical spectral analysis curve around a main peak at approximately 1.11 cycles/ky. This is because an oscillating function with a 900-year component/wavelength will result in a frequency of 1.11, as the frequency is inversely proportional to the wavelength.

The spectral analysis shows that there is correlation between the frequencies of the continental records at Burdukovo and the North Atlantic data. This supports the excellent correlation between the magnetic data and the grain size data of the Burdukovo site with the oxygen isotope data and the insolation curve from the North Atlantic as described in Chapter 5.4.

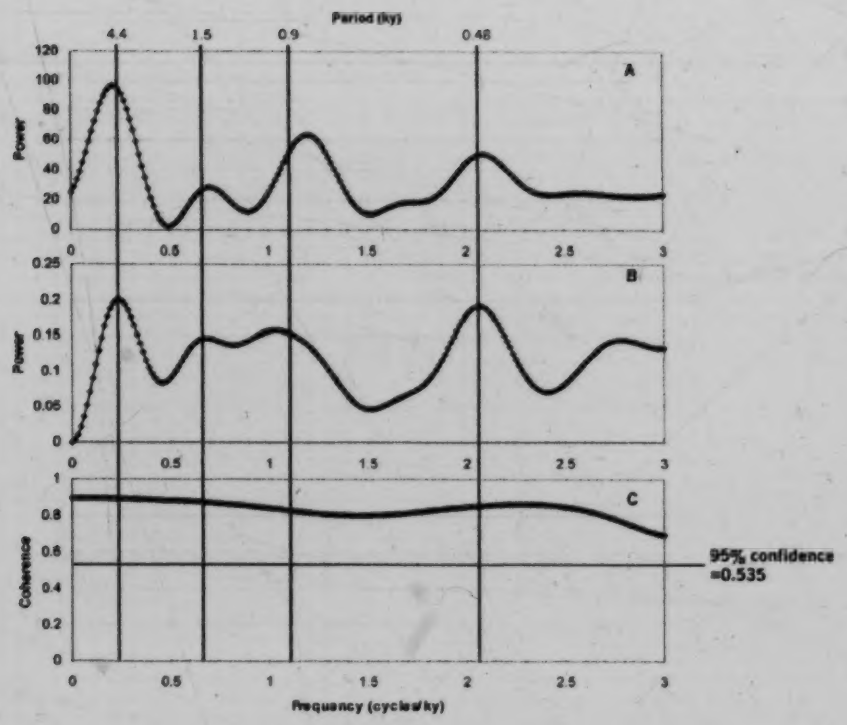

Figure 5.5.1 Comparison of the frequency analyses of **(A)** median grain size and **(B)** FD. The relation between median grain size and the FD can be seen in **(C)** the consistently high coherence between the two parameters.

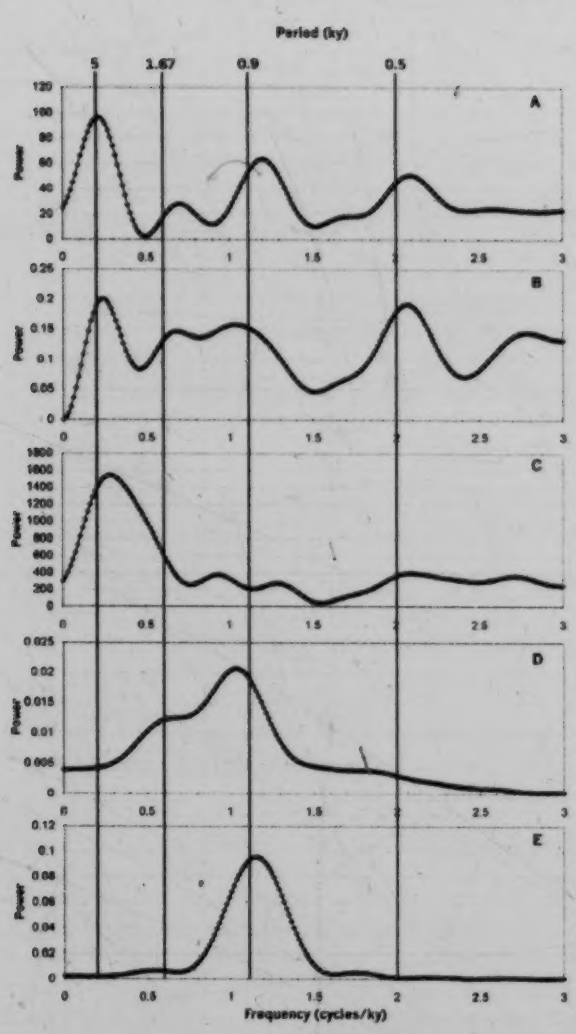

Figure 5.5.2 Comparison of spectral analysis performed on: **(A)** median grain size from the Selenga River valley loess/soil sequence, **(B)** FD of the loess/soil sequence from the Selenga River valley, **(C)** diatom concentrations from Lake Baikal from Morley et al. (2005), **(D)** smoothed and normalised oxygen isotope data from GISP2 ice core from Schulz and Paul (2002); original data from Grootes and Stuiver (1997), and **(E)** summer insolation curve with a 900-year component from Schulz and Paul (2002).

Chapter 6 Discussion

Over the last 10ky the climate in southern Siberia has gone through cycles of cool, windy periods followed by warm, calm, moist periods. During the warmer times, the calmer winds transported smaller grains from the surrounding hills and deposited them in the Selenga River valley. The weaker winds also transport less magnetic material into the valley initially giving them a low magnetic susceptibility. The warmer temperatures and more humid conditions allow for soil forming processes to occur at a faster rate than deposition. This results in the formation of soil horizons. During soil forming processes, bacterial utilize the Fe in the larger grain sediment such as goethite or limonite during metabolization and produce superparamagnetic magnetite (microscopic magnetite), as indicated by high temperature scans and magnetic moment studies. This causes an increase in magnetic susceptibility in the soil horizons. In typical soil units such as those found in Chinese loess deposits the magnetic susceptibility is much high than in the loess units. For soil units in a wind vigour model, the magnetic susceptibility of the soil units (due to bacterial activity), can be similar to the magnetic susceptibility in loess units (due to input of magnetic material from the source area). Magnetic susceptibility caused by bacterial activity can be differentiated from original magnetic susceptibility by measuring both the high and low frequency magnetic susceptibility. The frequency dependence percentage (FD) of the magnetic susceptibility can then be calculated. The magnetite produced during soil formation exhibits a high FD because the smaller magnetite grain size is able to react to an alternating field at the high frequency while large grains are not able to respond as readily.

During the cold windy periods, loess horizons were deposited along the river valley. Because of the stronger winds, sediments of a larger grain size were able to be transported from the surrounding hills and deposited in the valley. As well, the increased winds caused the rate of deposition to increase to the point where any soil forming processes that may have been occurring, could not keep up with the rate of sedimentation. The Stronger winds were also able to transport more heavy magnetic particles. This resulted in the loess units having a magnetic susceptibility comparable to that of soil units despite a much lower rate of soil formation. These loess horizons are characterised by a larger grain size and a low FD magnetic susceptibility.

The style of deposition at work at the Burdukovo study site is called a wind vigour model and makes the section an atypical loess/soil sequence. It also means that the low frequency magnetic susceptibility is not as reliable indicator of climate change as it is in typical loess/soil sequences. This is because the deposition of magnetic material in the study area is not consistent. Weaker winds cannot carry heavy magnetite grains as far as the stronger winds so less magnetite reaches the study site from the source area. This is the reason that the FD is used in this study as a proxy for climate change. The wind vigour model also allows for the grain size analysis to be used as an indicator of relative wind strength. This allowed for the correlation of grain size with FD because wind strength increases, thereby grain size also increases, during the colder glacial periods that also result in loess depositional units that have a lower frequency dependent magnetic susceptibility.

In the Selenga River valley the three sampled trenches were correlated to produce a complete section. The complete and correlated section shows 9 distinct individual soil

profiles. The complete section was then correlated to the FD and the grain size. The soil horizons corresponded to highs in FD and lows in median grain size as expected. The loess units should then correspond to lows in the FD and highs in the median grain size, which they do. Once the stratigraphy, FD and grain size were correlated, an age model was applied to help determine rate of deposition and from that the frequency of the warming and cooling trends could be calculated. For the age model, the rate of deposition was taken to be linear between sequential calibrated dates. For the entire section, the maximum rates of deposition were calculated. What this resulted in was an elevated rate of sedimentation for the last 3.78 ky, as the thickest section from the main buried soil to the present day surface occurred at the thickest part of a paleo-depression. Because the deposition was occurring in a paleo-depression, the rate of deposition is exaggerated to a value of 69.5 cm/ky. If the rate had been calculated at the plateau that occurs in trench 3, the resulting rate of deposition would be approximately 16.5 cm/ky. The reason for using a larger depositional rate is that it allowed for more data points in the same time frame as a smaller depositional rate. Another reason is that there are units above the main buried soil that are represented in trench 1 that are not observed in trench 3. By using the thickness of units in trench 1 to determine for the rate of deposition, we can more easily observe the warming and cooling periods that have occurred since the warm period responsible for the main buried soil. Once the age model was calculated and applied to the Burdukovo site, the results could be compared to data from other sites. In marine and near marine settings the warm and cold trends are modelled using oxygen isotope data in both marine Foraminifera and glacial ice. In the North Atlantic the

warming and cooling trends can be characterised using ^{18}O data from the Greenland Ice Sheet.

The ^{18}O isotope has a higher vapour pressure than the ^{16}O isotope and will precipitate out more readily. This means that during colder periods, more ^{18}O will precipitate out over the oceans as the moist air moves northward. This means that the oceans will be enriched in ^{18}O during colder periods and glacial ice will become deficient in ^{18}O. In the GISP2 data, millennial scale warming and cooling trends are observed. These warming and cooling trends correlate very well with the warming and cooling trends observed at the Burdukovo site. The trends correlate well enough that a spectral analysis was performed on the data from the Burdukovo site and the GISP2 data from the North Atlantic to compare frequencies.

A spectral analysis was also performed for the insolation curve that was proposed by Loutre et al. (1992) and on the concentration of diatoms in Lake Baikal during the Holocene.

The results from all five of the frequency analyses are remarkably consistent and provides evidence that millennial scale cyclicity occurs globally. There is a noticeable difference between the studies in that the studies from Central Asia show a peak at a period of 5.0 ky. A likely explanation for this may be that our sample interval for the spectral analysis spanned just under 10 ky, which would mean that the peak at 5.0 ky is the result of a single data point. Also, the data from Morley et al. (2005) spanned approximately 15.7 ky. Another possibility is, that every third cycle in the 1.67 ky warming trend is more intense warming period in Central Asia that is not observed in the North Atlantic. This would result in a prominent peak at 0.2 cycles/ky that would

translate to a 5 ky period. There are slight differences between our calculated periods and those from the North Atlantic but this could be accounted for by slight differences in respective age models. In the end what is seen is that climate changes in the Selenga River closely follow the climate variability seen in marine environments from other parts of the world. The 0.9 ky cycle observed by Schulz and Paul (2002) is confirmed by our data. As well, the 1.5 ky cycle proposed by Bond et al. (1993) corresponds well with our 1.67 ky cycle. While it has been speculated that the cyclicity seen in the North Atlantic climate was a global occurence, the data from the Burdukovo site gives actual evidence that Holocene climate cyclicity is truly global.

The driving force behind these climate changes seen through the Holocene, could be insolation. Rahmstorf (2006) proposed that variability in solar radiation is a strong factor in causing the cyclic change in the thermohaline circulation, which in turn would drive the climate cyclicity in the North Atlantic. If the change in climate cause by insolation is strong enough it could also account for global Holocene climate changes observed at the Burdukovo site, as variability in solar radiation could not be restricted to the North Atlantic. Schulz and Paul however, believe that insolation on its own is not strong enough a factor to cause such strong climatic changes and propose that there is an amplifying factor that has yet to be accounted for, a factor that is working to increase the effect of insolation on climate change. However, because the climate changes can be observed in the Burdukovo site, a continental setting, the effect of insolation may be stronger than they suggest and perhaps an amplifying factor is not required.

Chapter 7 Conclusions

A previously unstudied Holocene loess/soil sequence in central Asia provides a continuous record of climate change for the last 10 ky. While Holocene records from other regions of the world are from marine or near marine settings, the deposit at the Burdukovo site is a purely continental record of climate cyclicity. The results from the Burdukovo site provide evidence that millennial scale cyclicity is global in nature. Both the magnetic study and grain size analysis from the Selenga River valley display millennial scale cyclicity that correlates with data from the North Atlantic. What the results from the study also show is that FD is a useful proxy for climate change in an atypical loess/soil sequences and that the grain size is a reliable indicator of relative wind strength. The combination of FD and grain size indicates the deposition and formation of the loess/soil sequence during the Holocene in the Selenga River valley is similar to a wind vigour model. While the magnetic profile at Burdukovo is does not show the same results as other wind vigour models, such as that at Kurtak or in Alaska, the wind is the primary mechanism driving deposition in the Selenga River valley. The wind is the controlling factor in both the grain size and the magnetic material being deposited. What the results from the magnetic moment study as well as the high temperature scan tell us, is that the magnetic mineral that is being deposited and produced through soil formation at the site is primarily magnetite with a trace amount of what is being interpreted as maghemite.

Bibliography

Balkwill, D.L., D. Maratea, R.P. Blakemore, Ultrastructure of a magnetotactic spirillum, *Journal of Bacteriology* 141: 1399-1408, 1980.

Beget, J.E., D.B. Stone and D.B. Hawkins, Paleoclimatic forcing of magnetic-susceptibility variations in Alaskan loess during the late Quaternary, *Geology* 18 (1): 40-43, 1990.

Bianchi, G.G. and I.N. McCave, Holocene periodicity in North Atlantic climate and deep-ocean flow south of Iceland, Nature 397 (6719): 515-517, 1999.

Boes, X., N. Piotrowska and N. Fagel, High-resolution diatom/clay record in Lake Baikal from grey scale, and magnetic susceptibility over Holocene and Termination I, *Global and Planetary Change* 46 (1-4): 299-313, 2005.

Bond, G., H. Heinrich, W. Broecker, L. Labeyrie, J. McManus, J. Andrews, S. Huon, R. Jantschik, S. Clasen, C. Simet, K. Tedesco, M Klas, G. Bonani and S. Ivy, Evidence for massive discharges of icebergs into the North-Atlantic Ocean during the last glacial period, *Nature* 360 (6401): 245-249, 1992.

Bond, G., B. Kromer, J. Beer, R. Muscheler, M.N. Evans, W. Showers, S. Hoffmann, R. Lotti-Bond, I. Hajdas and G. Bonani, Persistent solar influence on north Atlantic climate during the Holocene, *Science* 294 (5549): 2130-2136, 2001.

Bronk Ramsey, C., Radiocarbon Calibration and Analysis of Stratigraphy: The OxCal Program, *Radiocarbon* 37(2): 425-430, 1995.

Bronk Ramsey, C., Development of the Radiocarbon Program OxCal, *Radiocarbon* 43 (2A): 355-363, 2001.

Bronk Ramsey, C., J. van der Plicht and B. Weninger, 'Wiggle Matching' radiocarbon dates , *Radiocarbon* 43 (2A): 381-389, 2001.

Chlachula, J., M.E. Evans and N.W. Rutter, A magnetic investigation of a Late Quaternary loess/palaeosol record in Siberia, *Geophysical Journal International* 132: 128-132, 1998.

Evans M.E. and F Heller, "Environmental magnetism: principles and applications of enviromagnetics", (R. Dmowska, J.R. Holton and H.T. Rossby eds.), Amsterdam; Boston, Academic Press, 2003.

Forster, T. and F. Heller, Loess deposits from the Tajik depression (central Asia): Magnetic properties and paleoclimate, *Geophysical Journal International* 118: 501-512, 1994.

Grootes P.M. and M. Stuiver, Oxygen 18/16 variability in Greenland snow and ice with 10(-3)- to 10(5)-year time resolution, *Journal of Geophysical Research-Oceans* 102 (C12): 26455-26470, 1997.

Gupta A.K., D.M. Anderson and J.T. Overpeck, Abrupt changes in the Asian southwest monsoon during the Holocene and their links to the North Atlantic Ocean, *Nature* 421 (6921): 354-357, 2003.

Kravchinsky, V.A., V.S. Zykina and V.S Zykin, Magnetic indicator of global paleoclimate cycles in Siberian loess-paleosol sequences, Submitted to *Earth and Planetary Science Letters*, 2007.

Lagroix, F. and S. Banerjee, The regional and temporal significance of primary aeolian magnetic fabrics preserved in Alaskan loess, *Earth and Planetary Science Letters* 225, 379-395, 2004.

Liu, X.M., T.S. Liu, T.C. Xu, C, Liu and M.Y. Cheng, The primary study on magnetostratigraphy of a loess profile in Xifeng area, Gansu province, *Geophys. J. R. Astron. Soc.* 92, 345-348, 1988.

Liu, X.M., J. Shaw, T.S. Liu, F. Heller and Y. Baoyin, Magnetic mineralogy of Chinese loess and its significance, *Geophysical Journal International* 108: 301-308, 1992.

Loutre M.F., A. Berger, P. Bretagnon and P.L. Blanc, Astronomical frequencies for climate research at the decadal to century time scale, *Climate Dynamics* 7(4): 181-194, 1992.

Lovley, D.R., J.F. Stolz, G.L. Nord Jr and E.J.P. Phillips, Anaerobic production of magnetite by a dissimilatory iron-reducing mocroorganism, *Nature* 330, 252-254, 1987.

Morley, D.W., M.J. Leng, A.W. Mackay and H.J. Sloane, Late glacial and Holocene environmental change in the Lake Baikal region documented by oxygen isotopes from diatom silica, *Global and Planetary* 46: 221-233, 2005.

Paillard, D., L. Labeyrie and P. Yiou, Macintosh program performs time-series analysis, *Eos Trans. AGU* 77: 379, 1996.

Pansu M. and J Gautheyrou, "Handbook of Soil Analysis: Mineralogical, Organic and Inorganic Methods" Berlin Heidelberg: Springer-Verlag, 2006.

Rahmstorf, S., Thermohaline Ocean Circulation. In "Encyclopedia of Quaternary Sciences", (S. A. Elias editor), Amsterdam: Elsevier, 2006.

Reimer PJ, MGL Baillie, E Bard, A Bayliss, JW Beck, C Bertrand, PG Blackwell, CE Buck, G Burr, KB Cutler, PE Damon, RL Edwards, RG Fairbanks, M Friedrich, TP Guilderson, KA Hughen, B Kromer, FG McCormac, S Manning, C Bronk Ramsey, RW

Reimer, S Remmele, JR Southon, M Stuiver, S Talamo, FW Taylor, J van der Plicht, and CE Weyhenmeyer, IntCal04 terrestrial radiocarbon age calibration, 0-26 cal kyr BP, *Radiocarbon* 46: 1029-1058, 2004.

Sartori, M., F. Heller, T Forster, M. Borkovec, J. Hammann and E. Vincent, Magnetic Properties of loess grain size fractions from the section at Paks (Hungary), *Physics of the Earth and Planetary Interiors* 116: 53-64, 1999.

Schulz, M. and A. Paul, Holocene climate variability on centenial-to-millennial time scales: 1. Climate records from the North-Atlantic realm. *In* "Climate Development and History of the North Atlantic realm" (G. Wefer, W Berger, K.E Behre, and E. Jansen, eds.), pp. 41-54, Berlin Heidelberg: Springer-Verlag, 2002.

Shackleton, N.J., A. Berger and W.R. Peltier, An alternative astronomical calibration of the lower Pleistocene timescale based on ODP site 677, *Trans. Royal Society Edinburgh Earth Science* 81, 251-261, 1990.

Tsatskin, A., F. Heller, E.A. Hailwood, T.S. Gendler, J.Hus, P. Montgomery, M. Sartori, and E.I. Virina, Pedosedimentary division, rock magnetism and chronology of the loess/palaeosol sequence at Roxolany (Ukraine), *Palaeogeography, Palaeoclimatology, Palaeoecology* 143: 111–133, 1998.

Zhu, R. X., G. Matasova, A. Kazansky, V. Zykina, and J. M. Sun, Rock magnetic record of the last glacial–interglacial cycle from the Kurtak loess section, southern Siberia, *Geophysical Journal International* 152, 335–343, 2003.

Appendix

Table 1 Table of FD% values for each unit

Unit	Freq dep% Trench 1	Trench 3	Trench 4
16	0.93		
	1.08		
	0.86		
	1.32		
	1.25		
	1.54		
	0.84		
	0.74		
	0.80		
	0.65		
	0.76		
	0.32		
	0.37		
	0.37		
	0.39		
	0.89		
	0.48		
	0.88		
	0.81		
	0.75		
	0.84		
	0.76		
	0.54		
	0.54		
	0.62		
	0.38		
	0.36		
	0.04		
	0.50		
	0.53		
	0.46		
	1.01		
	0.37		
	0.85		
	0.70		
	0.39		
	0.39		
	0.71		
	0.15		
	0.13		
	0.38		
	0.33		
	0.56		
15	1.17		
	0.30		
	0.59		
	0.61		
	0.80		
	0.65		
	0.93		

Unit	Freq Dep (%) Trench 1	Trench 3	Trench 4
15	0.98		
	0.43		
	0.36		
	0.50		
	0.77		
	1.36		
14	2.83		
	2.00		
	1.85		
	1.03		
	0.96		
	0.51		
	0.52		
	0.73		
	0.29		
	0.49		
	0.47		
	0.94		
	1.47		
13	3.84		
	1.87		
	0.92		
	1.06		
	0.79		
	0.71		
	0.33		
	0.30		
	0.62		
	0.69		
	0.90		
	0.99		
12	1.05		
	0.64		
	0.31		
	0.38		
	0.13		
	0.34		
	0.39		
	0.61		
	0.43		
	0.66		
	0.60		
	0.55		
	2.82		
	1.44		
11	4.61	1.48	0.40
	4.61	1.57	0.90
	5.32	2.41	0.39

Unit	Freq Dep (%) Trench 1	Trench 3	Trench 4
11	5.10	2.56	0.66
	4.48	2.47	
	4.44	2.35	
	3.41	1.69	
	2.74	1.72	
	1.67	1.07	
	1.88	0.99	
	0.86	1.09	
	0.28	1.53	
	1.02	1.29	
	1.38	1.45	
	1.19	1.11	
	1.12	0.81	
	0.77	0.36	
	1.13		
	0.80		
	0.72		
	0.81		
	0.55		
10		0.73	
		0.68	
		1.21	
		0.47	
		0.34	
		0.29	
		0.18	
		0.47	
9		1.31	
		0.59	
		0.54	
		0.57	
		0.63	
		0.59	
		0.88	
		1.78	
8		0.92	
		0.42	
		0.19	
		0.62	
		0.70	
		0.20	
		0.32	
		0.76	
7		1.51	
		0.82	
		0.49	
		0.35	
		0.57	

Unit	Freq Dep (%) Trench 1	Trench 3	Trench 4
6		0.00	
		0.03	
		0.16	
		0.71	
		0.18	
		0.22	
		0.38	
		0.27	
5		0.55	1.35
		0.37	2.01
		1.79	1.41
		0.85	1.64
		1.79	0.57
		0.78	0.52
		0.95	0.31
			0.85
			0.18
			0.70
			0.44
			0.86
			0.41
			0.34
			0.55
4		2.55	0.69
		2.13	0.44
		1.73	1.56
		1.30	1.80
		1.85	
		0.62	
3		1.95	1.60
		1.40	1.75
		1.14	1.42
		1.23	1.45
		1.16	1.12
		1.15	1.43
		1.03	1.56
			2.06
			2.12
			1.53
			2.42
			1.49
			1.39
			1.31
			1.22
			0.88
			0.78
			0.45
			0.48

Unit	Freq Dep (%) Trench 1	Trench 3	Trench 4
3			0.99
			0.61
			1.00
			0.63
			0.92
			0.74
			0.45
			0.81
			0.82
			0.79
			0.80
			0.54
			0.72
			0.62
			0.50
			0.59
			0.31
			0.68
			0.56
			0.83
			0.94
			0.64
			0.51
			0.70
			0.28
			0.67
			0.57
			0.33
			0.47
2			0.64
			0.47
			0.65
			0.60
			0.51
			0.44
			0.53
			0.27
			0.58
			0.30
			0.51
			0.77
			0.65
			0.48
			0.26
			0.42
			0.46
			0.45
			0.38

Unit	Freq Dep (%) Trench 1	Trench 3	Trench 4
2			0.04
			0.33
			0.76
			0.45
			1.17
			0.30
			0.53
			0.45
			0.41
			0.40
			0.45
1	fluvial sand & gravel, no data		

Table 2 Final Grainsize Analysis Data for Burdukovo Trench 1

Depth	Median grain	cummulative %										
(m)	size (um)	< 0.98 (um)	2-0.98 (um)	5-2 (um)	10-5 (um)	20-10 (um)	50-20 (um)	100-50 (um)	250 - 100 (um)	500 - 250 (um)	1 (mm) - 500 (um)	>1 (mm)
0.12	35.66	11.203	13.983	19.461	24.613	29.683	57.730	81.771	81.836	82.485	99.967	100.000
0.19	31.78	10.817	13.993	19.488	25.068	31.335	65.675	85.849	99.602	100.000	100.000	100.000
0.25	25.26	11.413	15.456	23.185	31.272	39.989	74.137	89.863	89.872	90.572	99.980	100.000
0.32	31.13	9.882	13.781	19.040	24.842	33.002	70.628	90.665	90.739	90.908	99.952	100.000
0.37	35.16	10.340	13.331	18.287	24.183	30.592	60.758	85.454	99.557	99.977	100.000	100.000
0.48	32.74	11.274	14.309	19.252	24.803	31.740	64.348	86.722	86.722	87.223	99.942	100.000
0.62	29.73	11.768	15.118	20.187	26.524	35.577	69.343	90.527	99.799	100.000	100.000	100.000
0.68	45.61	9.044	10.778	12.586	14.621	16.430	44.090	75.367	99.348	100.000	100.000	100.000
0.77	29.21	11.840	14.461	18.438	23.409	33.261	73.573	90.384	99.353	100.000	100.000	100.000
0.89	19.51	11.056	17.015	26.171	35.326	43.445	68.493	86.372	98.643	100.000	100.000	100.000
0.95	34.97	10.921	13.038	16.340	20.065	26.076	62.565	84.662	98.971	100.000	100.000	100.000
1.01	21.07	15.633	19.589	26.934	34.751	45.864	82.781	94.176	99.726	100.000	100.000	100.000
1.1	41.72	10.078	10.768	13.102	14.746	17.133	32.145	53.044	53.045	62.111	99.943	100.000
1.2	33.06	13.934	17.135	21.560	24.761	31.728	71.082	94.148	94.148	94.171	99.978	100.000
1.25	32.35	13.806	16.167	19.982	23.979	30.609	70.846	90.828	99.672	100.000	100.000	100.000
1.34	37.08	10.689	13.447	17.757	21.464	26.722	61.719	86.200	99.779	100.000	100.000	100.000
1.41	34.69	14.646	16.803	20.217	22.823	28.484	67.841	89.855	99.937	100.000	100.000	100.000
1.52	19.05	21.166	25.940	32.515	38.459	45.935	75.387	90.068	90.068	90.452	99.964	100.000
1.57	36.23	9.152	10.692	14.455	18.133	25.318	60.387	85.535	100.000	100.000	100.000	100.000
1.66	42.89	8.643	12.661	14.632	15.769	17.892	47.232	75.815	99.863	100.000	100.000	100.000
1.77	40.72	12.512	14.350	18.025	18.637	21.699	57.749	87.498	100.000	100.000	100.000	100.000
1.88	8.11	23.027	28.880	40.873	50.852	61.022	82.802	95.947	100.000	100.000	100.000	100.000
1.92	19.47	19.589	25.457	33.500	38.895	47.885	77.505	94.634	99.974	100.000	100.000	100.000
1.98	40.19	11.287	12.774	15.574	18.287	23.186	56.960	87.496	100.000	100.000	100.000	100.000
2.08	47.87	8.423	10.219	11.582	12.635	14.121	33.260	61.936	99.649	100.000	100.000	100.000
2.16	47.7	10.510	12.201	14.617	16.671	18.724	32.013	60.401	99.449	100.000	100.000	100.000
2.44	42.57	9.802	10.982	12.615	14.794	18.242	58.630	90.758	100.000	100.000	100.000	100.000
2.53	13.04	14.411	17.537	26.044	37.938	52.089	71.535	86.814	99.017	100.000	100.000	100.000
2.61	18.22	17.702	21.259	28.210	35.081	41.548	62.079	80.832	98.212	100.000	100.000	100.000
2.7	30.36	17.007	19.478	24.057	27.182	31.325	52.039	72.680	98.296	100.000	100.000	100.000
2.77	37.34	14.924	18.042	21.012	23.982	27.323	49.300	74.247	99.669	100.000	100.000	100.000
2.83	8.04	25.106	30.792	39.278	45.926	52.487	73.481	87.478	99.218	100.000	100.000	100.000
2.96	4.56	23.529	30.445	43.348	51.950	60.553	74.974	84.335	98.335	99.836	100.000	100.000
3.01	4.66	26.115	30.794	38.342	43.851	48.833	63.324	75.476	75.527	77.017	99.996	100.000
3.08	4.48	21.671	32.186	47.822	59.801	69.859	84.032	91.438	99.377	100.000	100.000	100.000
3.13	3.41	29.955	39.323	55.910	69.863	83.134	94.550	97.575	99.751	99.978	100.000	100.000
3.23	2.92	29.988	41.925	60.075	71.617	82.665	95.588	98.646	99.596	99.849	100.000	100.000
3.33	4.1	31.908	38.789	53.048	64.615	78.774	95.626	99.714	100.000	100.000	100.000	100.000
3.43	4.28	29.921	38.470	51.989	63.718	77.536	95.627	99.405	99.954	99.990	100.000	100.000
3.7	5.66	26.257	34.976	47.659	59.251	74.609	94.723	99.082	99.941	100.000	100.000	100.000
3.84	8.07	18.062	25.307	40.193	54.285	70.362	93.585	99.242	100.000	100.000	100.000	100.000
4	9.05	21.388	28.252	39.990	51.728	68.241	94.503	99.477	100.000	100.000	100.000	100.000

Table 3 Final Grainsize Analysis Data for Burdukovo Trench 3

Depth (m)	Median grain size (um)	Median grain cummulative % < 0.98 (um)	2-0.98 (um)	5-2 (um)	10-5 (um)	20-10 (um)	50-20 (um)	100-50 (um)	250 - 100 (um)	500 - 250 (um)	1 (mm) - 500 (um)	>1 (mm)
0.06	36.62	5.938	11.796	16.691	21.906	27.604	54.565	80.243	99.489	99.985	99.985	100.000
0.13	32.16	11.067	14.312	19.887	25.379	31.453	61.408	83.209	99.424	99.944	99.944	100.000
0.21	32.53	12.065	13.584	20.081	25.143	31.640	62.183	84.373	99.467	99.984	99.984	100.000
0.33	33.66	6.439	10.071	17.831	23.197	29.141	61.172	82.553	99.262	99.973	99.993	100.000
0.4	16.89	9.016	12.641	21.749	34.111	50.934	80.026	92.946	99.901	100.000	100.000	100.000
0.48	9.11	12.916	18.753	34.348	49.847	66.112	88.501	95.676	99.891	100.000	100.000	100.000
0.53	31.49	7.400	9.250	14.398	22.602	32.174	56.546	80.435	99.639	100.000	100.000	100.000
0.58	25.63	7.530	9.853	15.941	23.871	34.765	59.517	80.103	99.104	100.000	100.000	100.000
0.62	22.98	8.379	12.050	18.195	25.776	36.550	63.124	79.803	99.052	100.000	100.000	100.000
0.67	35.53	8.125	10.860	15.503	20.892	28.104	58.198	82.903	98.595	100.000	100.000	100.000
0.74	44.38	4.219	5.970	9.472	13.691	18.307	47.281	79.598	99.746	100.000	100.000	100.000
0.79	48.37	7.021	8.034	10.351	12.522	14.621	38.218	72.382	99.933	100.000	100.000	100.000
0.84	33.77	8.778	12.148	18.177	24.295	30.945	65.348	88.668	99.915	100.000	100.000	100.000
0.92	36.67	9.386	11.566	15.169	18.582	25.029	69.114	94.807	99.953	100.000	100.000	100.000
0.99	31.28	7.755	10.874	16.935	24.066	33.425	66.851	89.134	99.884	100.000	100.000	100.000
1.04	42.27	9.435	11.166	14.195	16.965	21.033	54.703	86.555	99.895	100.000	100.000	100.000
1.19	10.76	13.033	18.132	29.371	45.142	64.974	83.012	94.439	99.912	100.000	100.000	100.000
1.24	45.31	7.202	9.932	14.253	18.651	23.199	42.381	75.815	99.213	99.958	100.000	100.000
1.31	53.54	5.878	6.868	8.229	9.405	10.889	27.224	61.872	98.776	100.000	100.000	100.000
1.37	56.07	6.212	7.946	9.150	10.642	11.413	20.177	48.155	95.900	99.735	100.000	100.000
1.43	42.98	5.331	6.643	8.201	10.005	14.024	52.076	82.010	99.822	99.993	100.000	100.000
1.53	44.91	4.957	6.609	8.169	9.730	13.493	54.706	91.788	99.895	100.000	100.000	100.000
1.62	25.73	10.700	15.645	25.048	32.992	38.099	58.284	81.062	99.618	100.000	100.000	100.000
1.71	39.22	8.520	10.274	12.362	15.285	21.800	55.295	83.526	99.869	100.000	100.000	100.000
1.8	9	14.881	21.192	34.754	49.447	64.234	84.107	94.185	99.837	100.000	100.000	100.000
1.85	50.36	5.537	7.817	10.504	13.354	15.960	40.226	81.430	99.899	100.000	100.000	100.000
1.91	5.46	18.281	26.786	46.631	64.326	80.065	94.533	97.759	99.454	99.856	99.984	100.000
1.97	4.94	19.607	28.925	48.921	65.519	79.690	94.056	97.065	98.854	99.398	99.690	100.000
2.04	3.43	25.198	35.859	58.925	74.238	83.445	93.330	96.916	99.437	99.926	99.971	100.000
2.1	2.52	29.104	43.162	68.900	80.087	86.324	95.629	98.995	99.904	99.993	100.000	100.000
2.14	12.73	18.190	24.679	35.102	44.737	58.404	87.508	98.324	99.991	100.000	100.000	100.000
2.24	2.83	25.910	40.205	67.901	84.082	91.925	97.782	99.271	99.857	99.964	100.000	100.000
2.29	4.5	22.999	32.786	51.087	64.691	78.294	93.562	97.868	99.452	99.935	99.978	100.000
2.39	5.15	20.891	30.595	48.912	63.268	78.120	95.051	99.011	99.713	99.826	99.826	100.000
2.47	8.1	17.249	25.675	40.842	54.225	70.086	93.184	99.132	99.972	100.000	100.000	100.000
2.54	8.36	16.081	23.874	39.264	53.175	68.072	91.650	98.654	99.907	99.989	100.000	100.000
2.61	10.34	14.690	21.538	35.235	48.932	65.904	92.306	99.254	99.970	100.000	100.000	100.000

Table 4 Final Grainsize Analysis Data for Burdukovo Trench 4

Depth	Median grain	cummulative %							250 -	500 -	1 (mm) -	1 (mm) -
(m)	size (um)	< 0.98 (um)	2-0.98 (um)	5-2 (um)	10-5 (um)	20-10 (um)	50-20 (um)	100-50 (um)	100 (um)	250 (um)	500 (um)	2 (mm)
0.06	39.91	10.300	13.438	18.668	22.691	26.554	51.900	80.466	99.360	99.985	99.985	100.000
0.13	28.99	16.728	20.416	26.164	31.225	37.144	63.565	85.782	99.409	99.949	99.949	100.000
0.21	33.99	11.651	15.282	23.556	27.440	32.590	59.861	84.431	99.622	99.952	99.952	100.000
0.33	31.44	14.790	18.641	24.241	29.492	35.531	65.548	87.514	99.571	100.000	100.000	100.000
0.4	22.28	15.674	19.794	27.408	35.021	43.261	70.579	89.567	99.545	99.968	100.000	100.000
0.48	35.21	13.463	14.818	17.077	19.517	25.390	68.851	90.356	99.684	99.986	100.000	100.000
0.53	33.92	11.343	13.773	18.045	22.243	27.841	51.704	73.653	98.022	99.943	100.000	100.000
0.58	31.56	13.291	15.784	20.519	24.838	31.235	61.888	83.071	99.068	100.000	100.000	100.000
0.62	30.66	15.138	18.273	24.095	29.111	35.830	66.105	89.574	99.608	100.000	100.000	100.000
0.67	28.05	13.090	17.001	23.147	28.574	35.438	57.467	79.816	99.873	100.000	100.000	100.000
0.74	39.66	13.129	14.126	18.280	22.518	27.919	53.594	83.092	99.516	99.987	99.987	100.000
0.79	38.1	13.842	15.845	20.399	24.405	29.778	62.289	91.065	99.834	100.000	100.000	100.000
0.84	28.01	12.949	15.704	23.234	31.132	39.856	71.906	91.834	99.873	100.000	100.000	100.000
0.92	44.17	11.725	13.101	15.138	17.284	19.761	31.211	55.046	95.568	99.829	99.989	100.000
0.99	39.74	10.985	13.417	15.933	18.616	23.564	56.101	83.858	99.927	100.000	100.000	100.000
1.04	39.17	12.637	14.862	18.066	21.270	26.699	60.250	88.996	99.925	100.000	100.000	100.000
1.19	25.8	13.094	18.599	25.604	31.526	38.031	64.720	83.402	99.575	99.996	99.996	100.000
1.24	28.39	16.758	20.740	27.294	31.193	36.660	60.893	82.961	99.359	99.949	100.000	100.000
1.31	24.66	16.117	20.512	26.617	31.338	37.687	63.083	81.397	97.811	98.386	98.432	100.000
1.37	12.34	20.242	25.512	32.956	39.397	47.343	69.928	83.646	99.551	99.914	99.955	100.000
1.43	11.5	17.397	22.993	31.997	41.614	52.105	74.835	87.424	99.329	99.755	99.815	100.000
1.53	37.21	14.459	16.462	19.598	23.082	28.395	60.710	87.102	99.936	100.000	100.000	100.000
1.62	4.43	25.247	34.088	51.083	63.068	74.562	92.245	98.237	99.980	100.000	100.000	100.000
1.71	30.05	14.035	17.049	20.911	25.903	35.040	73.189	94.194	99.984	100.000	100.000	100.000
1.8	36.62	7.602	13.172	16.973	20.509	26.697	62.322	88.400	99.853	99.907	99.907	100.000
1.85	19.21	20.141	22.023	32.188	39.152	47.717	75.387	94.116	99.957	100.000	100.000	100.000
1.91	39.79	10.676	13.843	17.371	20.266	25.061	60.889	90.475	100.000	100.000	100.000	100.000
1.97	5.77	28.051	35.738	47.717	60.694	80.360	97.431	99.826	99.987	99.987	99.987	100.000
2.04	1.83	36.539	52.512	85.257	95.839	98.036	99.833	99.833	100.000	100.000	100.000	100.000
2.1	3.31	27.038	37.601	57.855	69.969	80.048	92.549	96.910	99.439	99.942	100.000	100.000
2.14	4.7	21.430	30.080	49.588	65.445	77.746	92.257	96.101	99.551	99.971	100.000	100.000
2.24	2.79	26.865	39.460	67.014	79.118	87.187	94.666	98.405	99.674	99.957	100.000	100.000
2.29	4.42	22.759	32.456	52.247	67.981	81.537	95.588	98.953	99.874	100.000	100.000	100.000
2.39	4.99	16.014	19.671	49.425	65.241	80.662	96.280	98.850	99.788	99.948	100.000	100.000
2.47	5.62	19.186	28.033	47.417	61.831	77.438	96.624	99.407	99.838	99.924	100.000	100.000
2.54	9.27	11.938	20.991	36.609	51.432	69.239	94.707	99.482	99.934	99.982	100.000	100.000
2.61	11.33	12.585	21.139	34.511	46.703	62.336	89.866	98.321	99.961	100.000	100.000	100.000
4.25	36.24	0.609	0.794	0.996	1.223	1.508	2.828	4.201	8.459	12.805	14.856	18.138

Table 5 Magnetic moment measurements for Burdukovo samples. The inducing field that sample BD1-25 was exposed to was created using manually set coils and is therefore in a separate data set table

B (mT)	M (Am^2) BD1-25
0	8.57E-07
15.65	6.73E-06
19.35	9.66E-06
29.8	1.82E-05
38.4	2.46E-05
48.1	3.18E-05
62	3.92E-05
81.7	4.79E-05
93.5	5.40E-05
105.4	5.97E-05
150.7	7.01E-05
200.5	7.77E-05
281	8.12E-05
420	8.21E-05
710	8.31E-05
730	8.37E-05
0	8.37E-05
-8.85	6.60E-05
-14.65	5.32E-05
-25.25	3.48E-05
-34.3	2.13E-05
-46.5	6.23E-06
-56.6	-7.69E-06
-56.6	-8.83E-06
-65.7	-1.69E-05
-80	-2.82E-05
-95	-3.94E-05
-109.3	-5.15E-05
-127	-5.91E-05
-165	-7.13E-05
-214	-7.87E-05
-301	-8.33E-05
-504	-8.42E-05
-722	-8.48E-05

B (mT)	M (Am^2) BD1-230	BD1-260	BD3-40	BD3-55	BD4-200
0	2.07E-05	4.43E-05	2.94E-05	3.02E-05	2.00E-05
10	2.20E-05	4.62E-05	3.02E-05	3.09E-05	2.02E-05
20	2.23E-05	4.68E-05	3.08E-05	3.17E-05	2.05E-05
30	2.63E-05	4.95E-05	3.29E-05	3.36E-05	2.16E-05
40	3.32E-05	6.04E-05	4.06E-05	4.22E-05	2.72E-05
50	4.11E-05	7.28E-05	5.02E-05	5.16E-05	3.47E-05
60	5.02E-05	8.25E-05	5.95E-05	6.13E-05	4.19E-05
70	6.01E-05	8.98E-05	6.98E-05	7.15E-05	5.09E-05
80	7.13E-05	9.64E-05	7.97E-05	8.02E-05	5.87E-05
90	7.94E-05	1.01E-04	8.71E-05	8.70E-05	6.61E-05
100	8.80E-05	1.05E-04	9.51E-05	9.75E-05	7.83E-05
120	9.74E-05	1.07E-04	1.04E-04	1.09E-04	9.41E-05
140	8.37E-05	1.09E-04	1.03E-04	1.13E-04	1.03E-04
160	1.05E-04	1.07E-04	1.14E-04	1.22E-04	1.16E-04
180	1.03E-04	1.05E-04	1.13E-04	1.22E-04	1.18E-04
200	1.07E-04	1.06E-04	1.15E-04	1.25E-04	1.23E-04
220	1.09E-04	1.06E-04	1.19E-04	1.27E-04	1.27E-04
240	1.10E-04	1.06E-04	1.19E-04	1.28E-04	1.29E-04
260	1.08E-04	1.06E-04	1.20E-04	1.29E-04	1.30E-04
280	1.11E-04	1.06E-04	1.21E-04	1.30E-04	1.31E-04
300	1.11E-04	1.07E-04	1.22E-04	1.29E-04	1.30E-04
340	1.08E-04	1.07E-04	1.18E-04	1.29E-04	1.31E-04
380	1.12E-04	1.07E-04	1.21E-04	1.31E-04	1.30E-04
450	1.14E-04	1.08E-04	1.23E-04	1.31E-04	1.31E-04
600	1.15E-04	1.07E-04	1.25E-04	1.32E-04	1.31E-04
0	1.15E-04	1.07E-04	1.25E-04	1.32E-04	1.31E-04
-10	8.16E-05	9.04E-05	8.58E-05	9.53E-05	9.61E-05
-20	5.47E-05	5.26E-05	6.02E-05	6.82E-05	7.02E-05
-30	3.48E-05	1.89E-05	3.65E-05	4.31E-05	5.35E-05
-40	1.61E-05	-9.39E-06	1.51E-05	2.05E-05	3.70E-05
-50	-4.68E-06	-3.08E-05	-3.82E-06	1.78E-06	2.17E-05
-60	-1.50E-05	-4.68E-05	-1.93E-05	-1.50E-05	7.77E-06
-70	-2.94E-05	-6.09E-05	-3.24E-05	-2.90E-05	-4.55E-06
-80	-3.86E-05	-7.14E-05	-4.33E-05	-3.98E-05	-1.52E-05
-90	-4.91E-05	-8.15E-05	-5.58E-05	-5.31E-05	-2.79E-05
-100	-6.21E-05	-8.85E-05	-6.57E-05	-6.34E-05	-3.94E-05
-120	-6.94E-05	-9.47E-05	-7.63E-05	-7.53E-05	-5.32E-05
-140	-8.07E-05	-1.01E-04	-8.32E-05	-7.95E-05	-6.14E-05
-160	-9.12E-05	-1.07E-04	-8.63E-05	-8.08E-05	-6.30E-05
-180	-9.79E-05	-1.12E-04	-9.07E-05	-8.19E-05	-6.37E-05
-200	-1.02E-04	-1.14E-04	-9.26E-05	-8.24E-05	-6.70E-05
-220	-1.03E-04	-1.15E-04	-9.58E-05	-8.41E-05	-6.78E-05
-240	-1.07E-04	-1.17E-04	-9.69E-05	-8.65E-05	-6.99E-05
-260	-1.09E-04	-1.18E-04	-9.85E-05	-8.84E-05	-7.23E-05
-280	-1.08E-04	-1.19E-04	-1.00E-04	-9.09E-05	-7.34E-05
-300	-1.08E-04	-1.19E-04	-9.93E-05	-9.02E-05	-7.42E-05
-340	-1.09E-04	-1.19E-04	-9.98E-05	-8.99E-05	-7.39E-05
-380	-1.10E-04	-1.20E-04	-1.00E-04	-9.09E-05	-7.36E-05
-450	-1.09E-04	-1.20E-04	-1.01E-04	-9.16E-05	-7.64E-05
-600	-1.11E-04	-1.21E-04	-1.01E-04	-9.31E-05	-7.78E-05